circulate for 20 min. Recombinant human VEGF-A_{165} (100 ng ml^{-1}, 100 µl; PeproTech) or PBS was injected intradermally into the preshaved back skin. After 20 min, the mice were euthanized, and the area of skin that included the entire injection site was removed. For the Ang II infusion model, 100 µl of a 1% solution of Evans blue dye in saline was injected into the tail veins of male *Pik3c2a*$^{+/-}$ mice or *Pik3c2a*$^{+/+}$ littermates that had received Ang II infusion for 14 d prior (1.0 mg per kg body weight per day). Thirty minutes later, mice were perfused with saline in the right ventricle to remove intravascular Evans blue dye, and the heart and aorta tissues were excised. Evans blue dye was extracted from the tissues by incubation with formamide overnight at 55 °C, and Evans blue content was determined spectrophotometrically as described above.

Metabolic cell labeling, lipid extraction and phosphoinositide measurements. The amounts of cellular phosphoinositides were determined as described previously[61]. In brief, MEF were labeled for 48 h with 10 µCi ml^{-1} [^{3}H]-myo-inositol (Amersham Biosciences) in inositol-free DMEM containing 10% FBS. Labeling was quenched and lipids were extracted as described[61]. Dried lipids were deacylated and analyzed by HPLC using a Partisphere SAX column (Whatman). Radioactivity was measured in 0.5 ml fractions using a liquid scintillation counter.

Statistical analyses. Unless otherwise noted, data are presented as means ± s.e.m. and were analyzed using Prism 5 software (GraphPad Software Inc). Paired data were compared by two-tailed Student's *t* test or Mann-Whitney nonparametric *U* test. Comparisons between multiple groups were analyzed by one- or two-wayANOVA followed by Bonferroni's *post-hoc* test. For the Kaplan-Meier curves, *P* values were determined with a log-rank Mantel-Cox test. Results with $P < 0.05$ were considered statistically significant. The presented data represent at least three independent experiments.

Additional methods. Additional methodology is described in the online **Supplementary Methods**.

52. Sörensen, I., Adams, R.H. & Gossler, A. Dll1-mediated Notch activation regulates endothelial identity in mouse fetal arteries. *Blood* **113**, 5680–5688 (2009).
53. Bazigou, E. *et al.* Integrin-α9 is required for fibronectin matrix assembly during lymphatic valve morphogenesis. *Dev. Cell* **17**, 175–186 (2009).
54. Takakura, N. *et al.* Critical role of the TIE2 endothelial cell receptor in the development of definitive hematopoiesis. *Immunity* **9**, 677–686 (1998).
55. Benedito, R. *et al.* The Notch ligands Dll4 and Jagged1 have opposing effects on angiogenesis. *Cell* **137**, 1124–1135 (2009).
56. Compagni, A. *et al.* Control of skeletal patterning by ephrinB1-EphB interactions. *Dev. Cell* **5**, 217–230 (2003).
57. Oyama, O. *et al.* The lysophospholipid mediator sphingosine-1-phosphate promotes angiogenesis *in vivo* in ischemic hindlimbs of mice. *Cardiovasc. Res.* **78**, 301–307 (2008).
58. Du, W. *et al.* $S1P_2$, the G protein–coupled receptor for sphingosine-1-phosphate, negatively regulates tumor angiogenesis and tumor growth *in vivo* in mice. *Cancer Res.* **70**, 772–781 (2010).
59. Deng, G.G. *et al.* Urokinase-type plasminogen activator plays a critical role in angiotensin II–induced abdominal aortic aneurysm. *Circ. Res.* **92**, 510–517 (2003).
60. Okamoto, H. *et al.* Inhibitory regulation of Rac activation, membrane ruffling, and cell migration by the G protein-coupled sphingosine-1-phosphate receptor EDG5 but not EDG1 or EDG3. *Mol. Cell. Biol.* **20**, 9247–9261 (2000).
61. Sasaki, T. *et al.* Function of PI3Kγ in thymocyte development, T cell activation, and neutrophil migration. *Science* **287**, 1040–1046 (2000).

PLOS ONE

Origins and Properties of Dental, Thymic, and Bone Marrow Mesenchymal Cells and Their Stem Cells

Yukiya Komada[1], Toshiyuki Yamane[1], Daiji Kadota[1], Kana Isono[1], Nobuyuki Takakura[2], Shin-Ichi Hayashi[3], Hidetoshi Yamazaki[1]*

1 Department of Stem Cell and Developmental Biology, Mie University Graduate School of Medicine, Tsu, Japan, **2** Department of Signal Transduction, Research Institute for Microbial Disease, Osaka University, Suita, Japan, **3** Division of Immunology, School of Life Science, Faculty of Medicine, Tottori University, Yonago, Japan

Abstract

Mesenchymal cells arise from the neural crest (NC) or mesoderm. However, it is difficult to distinguish NC-derived cells from mesoderm-derived cells. Using double-transgenic mouse systems encoding *P0-Cre*, *Wnt1-Cre*, *Mesp1-Cre*, and *Rosa26EYFP*, which enabled us to trace NC-derived or mesoderm-derived cells as YFP-expressing cells, we demonstrated for the first time that both NC-derived (P0- or Wnt1-labeled) and mesoderm-derived (Mesp1-labeled) cells contribute to the development of dental, thymic, and bone marrow (BM) mesenchyme from the fetal stage to the adult stage. Irrespective of the tissues involved, NC-derived and mesoderm-derived cells contributed mainly to perivascular cells and endothelial cells, respectively. Dental and thymic mesenchyme were composed of either NC-derived or mesoderm-derived cells, whereas half of the BM mesenchyme was composed of cells that were not derived from the NC or mesoderm. However, a colony-forming unit-fibroblast (CFU-F) assay indicated that CFU-Fs in the dental pulp, thymus, and BM were composed of NC-derived and mesoderm-derived cells. Secondary CFU-F assays were used to estimate the self-renewal potential, which showed that CFU-Fs in the teeth, thymus, and BM were entirely NC-derived cells, entirely mesoderm-derived cells, and mostly NC-derived cells, respectively. Colony formation was inhibited drastically by the addition of anti-platelet–derived growth factor receptor-β antibody, regardless of the tissue and its origin. Furthermore, dental mesenchyme expressed genes encoding critical hematopoietic factors, such as interleukin-7, stem cell factor, and cysteine-X-cysteine (CXC) chemokine ligand 12, which supports the differentiation of B lymphocytes and osteoclasts. Therefore, the mesenchymal stem cells found in these tissues had different origins, but similar properties in each organ.

Citation: Komada Y, Yamane T, Kadota D, Isono K, Takakura N, et al. (2012) Origins and Properties of Dental, Thymic, and Bone Marrow Mesenchymal Cells and Their Stem Cells. PLoS ONE 7(11): e46436. doi:10.1371/journal.pone.0046436

Editor: Pranela Rameshwar, University of Medicine and Dentistry of New Jersey, United States of America

Received June 7, 2012; **Accepted** August 29, 2012; **Published** November 21, 2012

Funding: This work was supported by Grants-in-Aid for Scientific Research (B) (no. 21390489: HY) and Challenging Exploratory Research (no. 21659422: HY) from the Japan Society for the Promotion of Science and by funding from the Molecular Medical Science Institute, Takeda Pharmaceutical Co., Ltd. (HY). The funders had no role in study design, data collection and analysis, decision to publish, or preparation of the manuscript.

Competing Interests: The authors have declared that no competing interests exist.

* E-mail: yamazaki@doc.medic.mie-u.ac.jp

Introduction

All organs consist of layers of epithelial cells derived from one of the germ layers and mesenchymal cells derived from the neural crest (NC) or mesoderm. NC cells emerge from the dorsal region of the neural tube during embryogenesis and differentiate into melanocytes, neurons, glia, and mesenchymal cells, including osteoblasts, chondrocytes, adipocytes, odontoblasts, and perivascular cells [1,2]. NC cells participate in the organogenesis of the craniofacial area, including the tooth, heart, thymus, and bone marrow (BM) [2–7]. In particular, the cephalic NC supplies perivascular cells to the craniofacial area and thymus [8–10].

Mesoderm-derived cells have the potential to differentiate into osteoblasts, chondrocytes, and adipocytes, and contribute to the mesenchymal cells in the heart, thymus, and BM [2,4,11]. The craniofacial skeleton, including the mandible and maxilla, mainly develops from NC-derived cells; the skeleton outside this region mainly develops from mesoderm-derived cells [2,12]. Some mesoderm-derived cells contribute to the bones and cartilage of the cranial base and head muscles [13,14]. Mouse neck and shoulder skeleton is derived from mesenchymal cells that develop from both mesoderm-derived and NC-derived cells [15]. However, it is difficult to distinguish between NC-derived and mesoderm-derived cells.

Mesenchymal stem cells (MSCs) are long-term self-renewing cells, giving rise to one or more specialized cell types [16]. Friedenstein et al. first identified MSCs *in vitro* and termed them fibroblastic colony-forming units (CFU-F) [17]. They defined CFU-Fs as a BM cell population grown in a serum-containing medium that produces colonies of adherent fibroblast-like cells, which can differentiate into osteoblasts, chondrocytes, and adipocytes [17]. Although the origin of MSCs is unclear, they are present in both embryonic and adult tissues in mice and humans [16,18–20]. NC-derived multipotent cells in rodents can differentiate into neurons, glia, and myofibroblasts in the gut and sciatic nerve [21–23]; they have potentials similar to MSCs in the skin and BM [6,24–26].

To distinguish NC-derived cells from mesoderm-derived cells, we used double-transgenic mouse systems encoding *P0-Cre*, *Wnt1-Cre*, *Mesp1-Cre*, and *Rosa26EYFP*, which enabled us to trace NC- or mesoderm-derived cells as YFP-expressing cells [27–32]. *Wnt1* and *P0* are expressed in early migratory NC [5,30], and *Mesp1*, a transcription factor, is first observed at E6.5 (early gastrulation

stages), specifically in nascent mesoderm-derived cells [28]. In this study, we investigated the contributions of NC-derived and mesoderm-derived cells to the teeth, thymus, and BM using three transgenic mouse lines to establish the origin and properties of dental, thymic, and BM MSCs. CFU-F assays indicated that dental, thymic, and BM CFU-Fs comprise NC-derived and mesoderm-derived cells. We clarified the presence of cells in CFU-F progeny with the capacity for repeatable colony formation and retained multipotency.

Results

Contributions of NC-derived and mesoderm-derived cells to dental mesenchyme

We used *Wnt1-Cre*, *P0-Cre*, and *Mesp1-Cre* mice crossed with *Rosa26EYFP* mice (i.e., *Wnt1/YFP*, *P0/YFP*, and *Mesp1/YFP* mice, respectively) to investigate the contribution of NC-derived and mesoderm-derived cells to dental mesenchyme. Initially, we isolated hematopoietic cell-deprived YFP$^+$ and YFP$^-$ cells and examined the gene expression associated with the NC or mesoderm. Approximately two-thirds of YFP$^+$ cells from E9.5 *Wnt1/YFP* or *P0/YFP* embryos (i.e., Wnt1/YFP$^+$ and P0/YFP$^+$ cells) expressed p75NGFR (Fig. S1A). E9.5 Wnt1/YFP$^+$ (P0/YFP$^+$) and Mesp1/YFP$^-$ cells expressed NC-associated genes such as *AP2* and *Sox10* (Fig. S1B). Wnt1/YFP$^+$ cells in the dental mesenchyme, which were isolated from E13.5 and two-day-old mice, expressed NC-associated genes such as *p75*, *Sox10*, and *Krox20*, whereas Wnt1/YFP$^-$ cells expressed *Brachyury (T)*, a mesodermal gene (Fig. S1C). Therefore, we concluded that *Wnt1-Cre* and *P0-Cre* identified NC-derived cells.

To assess the proportion of Wnt1/YFP$^+$ cells in the dental mesenchymal cells, we prepared samples from mice that were devoid of blood cells. We found that approximately 90% of dental mesenchymal cells from E13.5 or two-day-old mice were Wnt1/YFP$^+$, whereas only approximately 7% were Mesp1/YFP$^+$ (Fig. 1A). This difference of approximately 10-fold was observed despite the presence of both NC-derived and mesoderm-derived cells in dental mesenchyme. Large numbers of E13.5 or two-day-old Wnt1/YFP$^+$ cells were observed in histological sections of the dental mesenchymal layer around the enamel organ and dental pulp, and Wnt1/YFP$^+$ cells were distributed throughout the mesenchyme, whereas only small numbers of Mesp1/YFP$^+$ cells were found in these locations (Fig. 1B, C).

Characteristics of dental mesenchymal cells and the origins of their CFU-Fs

We fractionated dental mesenchymal cells using three markers to compare their origins: CD31 (an endothelial marker), platelet-derived growth factor receptor-α (PDGFRα) (a mesenchymal cell marker), and PDGFRβ (a mesenchymal cell or perivascular cell marker). Among the E13.5 dental mesenchymal cells, Mesp1/YFP$^+$ expressed CD31 but Wnt1/YFP$^+$ cells rarely expressed it. In contrast, Wnt1/YFP$^+$ cells expressed PDGFRα and PDGFRβ but Mesp1/YFP$^+$ rarely expressed these markers(Fig. 1A). *Wnt1-Cre* and *Mesp1-Cre* were indicators of reciprocally separable cell populations. PDGFRα- and PDGFRβ-expressing cells were found only in the Mesp1/YFP$^-$ cell fraction. Dental pulp cells from two-day-old and four-week-old mice produced similar results (Fig. 1A). We also examined the expression of the endothelial cell markers CD34, FLK1, and Sca1 (an MSC marker). Sca1 was expressed in Mesp1/YFP$^+$ cells from two-day-old mice (Fig. 1A). All four-week-old Mesp1/YFP$^+$ cells expressed CD31, whereas 42% and 53% expressed CD34 and FLK1, respectively (Fig. S2). Similarly, histological sections revealed that Wnt1/YFP$^+$ cells in the perivascular lining of two-day-old mice expressed α-SMA, but not CD31 (Fig. 1D′–D′″). In 2-day-old mice, Mesp1/YFP$^+$ dental mesenchymal cells were located in the inner layer of blood vessels and expressed CD31, but not α-smooth muscle actin (α-SMA)(Fig. 1E′–E′″). Thus, NC-derived and mesoderm-derived cells may contribute to α-SMA$^+$ perivascular cells and CD31$^+$ endothelial cells, respectively.

We performed CFU-F assays to determine the origin of dental MSCs, which are functional assays for measuring MSCs *in vitro* (Fig. 2A). We used unfractionated cells, including YFP$^+$ and YFP$^-$

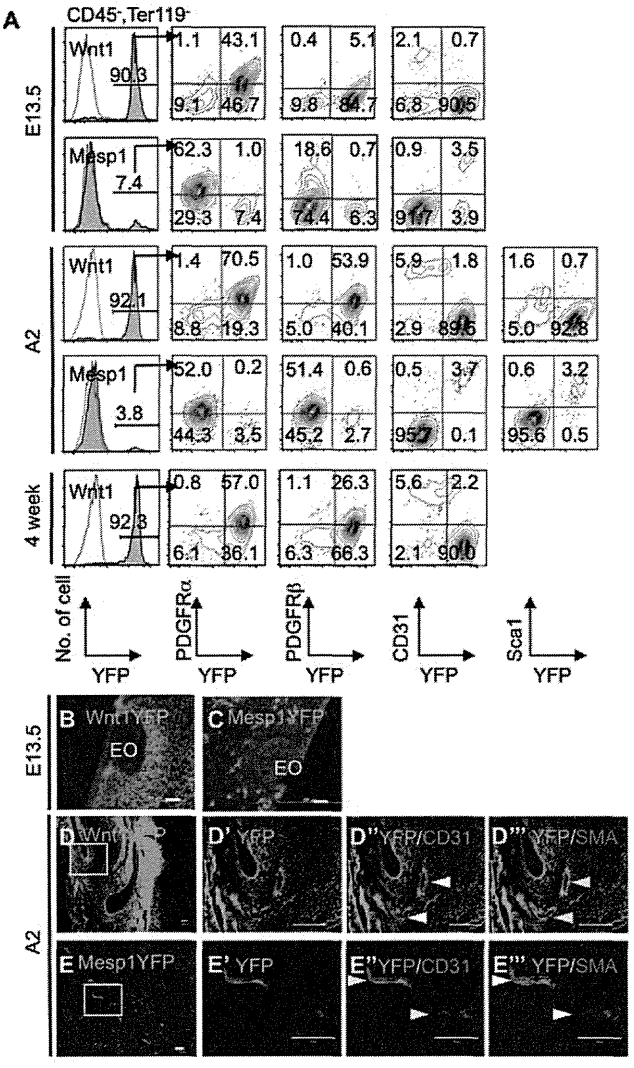

Figure 1. Origins and characteristics of NC-derived and mesoderm-derived cells of the dental mesenchyme. (A) Expression of YFP and cell surface molecules by dental mesenchymal cells prepared from E13.5, 2-day-old, and 4-week-old *Wnt1-Cre/YFP* and *Mesp1-Cre/YFP* mice. The proportions of YFP$^+$ cells in the CD45$^-$ and Ter119$^-$ fractions are indicated. (B, C) Immunohistochemistry of YFP in the mandibular molars of E13.5 *Wnt1-Cre/YFP* (B) and *Mesp1-Cre/YFP* embryos (C). EO, enamel organ. (D, E) Immunohistochemistry of YFP, CD31, and α-SMA in the mandibular incisors of 2-day-old *Wnt1-Cre/YFP* (D) and *Mesp1-Cre/YFP* mice (E). High-magnification views (D′–D′″and E′–E′″) of the boxed areas in (D) and (E), respectively. Yellow and white arrowheads indicate positive cells for each antibody to indicate the presence or absence of YFP$^+$ cells, respectively. Scale bars = 50 μm. All experiments were repeated in duplicate and one representative experiment is presented.
doi:10.1371/journal.pone.0046436.g001

cells from E13.5 *Wnt1/YFP* or *Mesp1/YFP* embryos, but all colonies comprised Wnt1/YFP$^+$ or Mesp1/YFP$^-$ cells (Fig. 2B, C). Using unfractionated dental pulp cells from two-day-old mice, we found that all colonies were Wnt1/YFP$^+$, except one, and that all consisted of Mesp1/YFP$^-$ cells (Fig. 2C). Four-week-old *Mesp1/YFP* and *Wnt1/YFP* mice yielded similar results (Table S1).

To estimate the self-renewal activity of CFU-Fs, we examined the capacity for repeatable colony formation (secondary or tertiary CFU-F assays). Cells from primary colonies were used to detect secondary CFU-Fs. The frequency of secondary colony formation (0.37%–2.00%) was approximately 10 times higher than that of primary colony formation (0.06%–0.29%) (Table S1). These results suggest that dental CFU-Fs contain self-renewing MSCs. All secondary colonies were Wnt1/YFP$^+$, but only one secondary colony from four-week-old *Mesp1/YFP* mice was composed of Mesp1/YFP$^+$ cells in one of two independent experiments (Table S1, Exp. 1). The YFP$^+$ cells from *Mesp1/YFP* mice exhibited proliferative capacity. However, the frequency of Mesp1/YFP$^+$ colony formation was very low in the tertiary CFU-F assays (0.1%; 2/2,000 cells) compared with Wnt1/YFP$^+$ colonies (Fig. S3A).

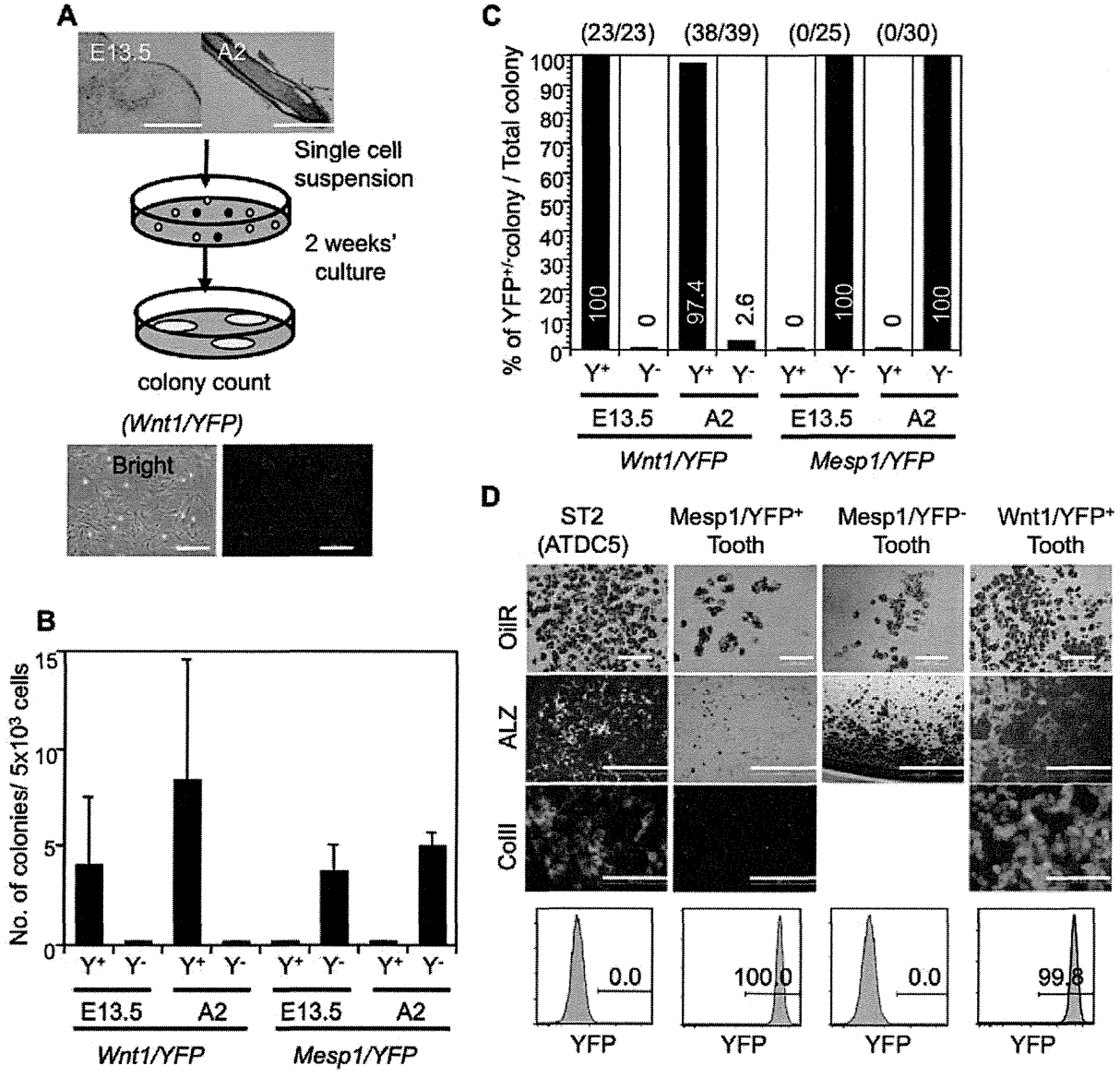

Figure 2. CFU-F assays and differential potential of dental mesenchymal cells of *Wnt1-Cre/YFP* and *Mesp1-Cre/YFP* mice. (A) Protocol of the CFU-F assays and fibroblastic colonies obtained from *Wnt1-Cre/YFP* mice. Scale bars, 200 μm. (B) Numbers of colonies induced from dental mesenchymal cells including both YFP$^+$ and YFP$^-$ cells of E13.5 and 2-day-old *Wnt1-Cre/YFP* and *Mesp1-Cre/YFP* mice. Values represent the mean (SD) of triplicate cultures of two independent experiments. Y$^+$, YFP$^+$ colonies; Y$^-$, YFP$^-$ colonies. (C) Percentages of YFP$^+$ and YFP$^-$ colonies induced from dental mesenchymal cells of *Wnt1-Cre/YFP* and *Mesp1-Cre/YFP* mice. Figures within parentheses indicate the number of YFP$^+$ colonies of the total number of colonies. Values represent percentages and colony numbers of triplicate cultures of two independent experiments ($n = 6$/group). (D) Differentiation potential of NC-derived and mesoderm-derived dental mesenchymal cells into adipocytes, osteoblasts, and chondrocytes. Cells from YFP$^+$ or YFP$^-$ colonies using dental mesenchymal cells from *Wnt1-Cre/YFP* or *Mesp1-Cre/YFP* mice were collected using a cell sorter. YFP expression in each cell preparation is shown in the lower panel. The cultured cells were stained with oil red O (OilR), alizarin red (ALZ), and anti-type II collagen (Col II) antibody to detect adipocytes, osteoblasts, and chondrocytes, respectively. ST2 and ATDC5 cells were the positive controls. The experiments were repeated twice and one representative experiment is presented. Scale bars, 200 μm in OilR and Col II and 1 mm in ALZ.
doi:10.1371/journal.pone.0046436.g002

Mesp1/YFP$^+$ cells recovered from primary or secondary colonies expressed PDGFRβ, but scarcely expressed CD31, which was similar to Wnt1/YFP$^+$ cells (Fig. S3B, C). Thus, CFU-Fs containing dental MSCs in the dental mesenchyme were generated mainly from NC-derived cells and rarely from mesoderm-derived cells.

Dental CFU-Fs with the potential for differentiation into osteoblasts, adipocytes, and chondrocytes are derived from NC

CFU-Fs are defined as cells with the potential for differentiation into osteoblasts, adipocytes, and chondrocytes *in vitro*. To assess whether colonies induced from dental mesenchymal cells could differentiate into these types, we performed CFU-F assays using two-day-old or four-week-old *Wnt1/YFP* and *Mesp1/YFP* mice. Cell suspensions prepared from YFP$^+$ colonies were cultured using reagents to induce their differentiation. Because Mesp1/YFP$^+$ dental mesenchymal cells formed few colonies in the CFU-F assays, Mesp1/YFP$^+$ cells were sorted and cultured. The cultured cells were stained with ALZ, OilR, or anti-type II collagen (Col II) antibody after 2–3 weeks to detect osteoblasts, adipocytes, and chondrocytes, respectively. Large numbers of ALZ$^+$, OilR$^+$, and Col II$^+$ cells were induced from Wnt1/YFP$^+$ dental mesenchymal cells (Fig. 2D). P0/YFP$^+$ dental mesenchymal cells also produced similar results. However, OilR$^+$ cells and a small number of ALZ$^+$ cells, but no Col II$^+$ cells, were induced from Mesp1/YFP$^+$ dental mesenchymal cells. In contrast, large numbers of ALZ$^+$ and OilR$^+$ cells were induced from Mesp1/YFP$^-$ cells (Fig. 2D). These results indicate that dental CFU-Fs with MSC properties were present in the dental pulp and were derived only from NC.

Roles of PDGFRs in CFU-Fs from dental mesenchymal cells

It is known that PDGFRs are expressed on MSCs, and PDGFRα$^+$ and PDGFRβ$^+$ cells were found among Wnt1/YFP$^+$ dental mesenchymal cells. PDGF is related to the CFU-F colony size when culturing BM cells in serum-deprived conditions [33], but the roles of PDGFRs in dental mesenchymal cells are unclear. We assessed their roles in colony formation using inhibitory antibodies against PDGFRα (anti-PDGFRα) and/or PDGFRβ (anti-PDGFRβ). We classified the colonies as either large (>50 cells) or small (approximately 8–50 cells). Anti-PDGFRα alone had little effect on colony formation, whereas anti-PDGFRβ decreased the number of large colonies to 15% of that observed in the presence of the isotype control or anti-PDGFRα in the primary CFU-F assay (Table S2, Fig. 3A). The total colony number observed in the presence of anti-PDGFRβ was 55% of that observed in the presence of anti-PDGFRα or the isotype control (Table S2, Fig. 3A). Similarly, in the secondary CFU-F assay, the number of total and large colonies formed in the presence of anti-PDGFRβ were 65% and 33%, respectively, of those observed in the presence of the isotype control (Fig. 3B). Thus, signaling by PDGFRβ is important for maintaining dental CFU-Fs. However, we cannot rule out the possibility that PDGFRβ signaling promoted the proliferation of CFU-F descendants (Fig. 3A, B), because anti-PDGFRβ affected the number of large colonies rather than the total number of colonies. To clarify this issue, we performed a primary CFU-F assay in the presence of anti-PDGFRβand/or anti-PDGFRα, and a secondary CFU-F assay in the absence of these antibodies. Cells prepared from colonies in the primary CFU-F assay treated only with anti-PDGFRβ or with both anti-PDGFRα and anti-PDGFRβ produced 50% or 0% of cells prepared from colonies observed in the presence of the

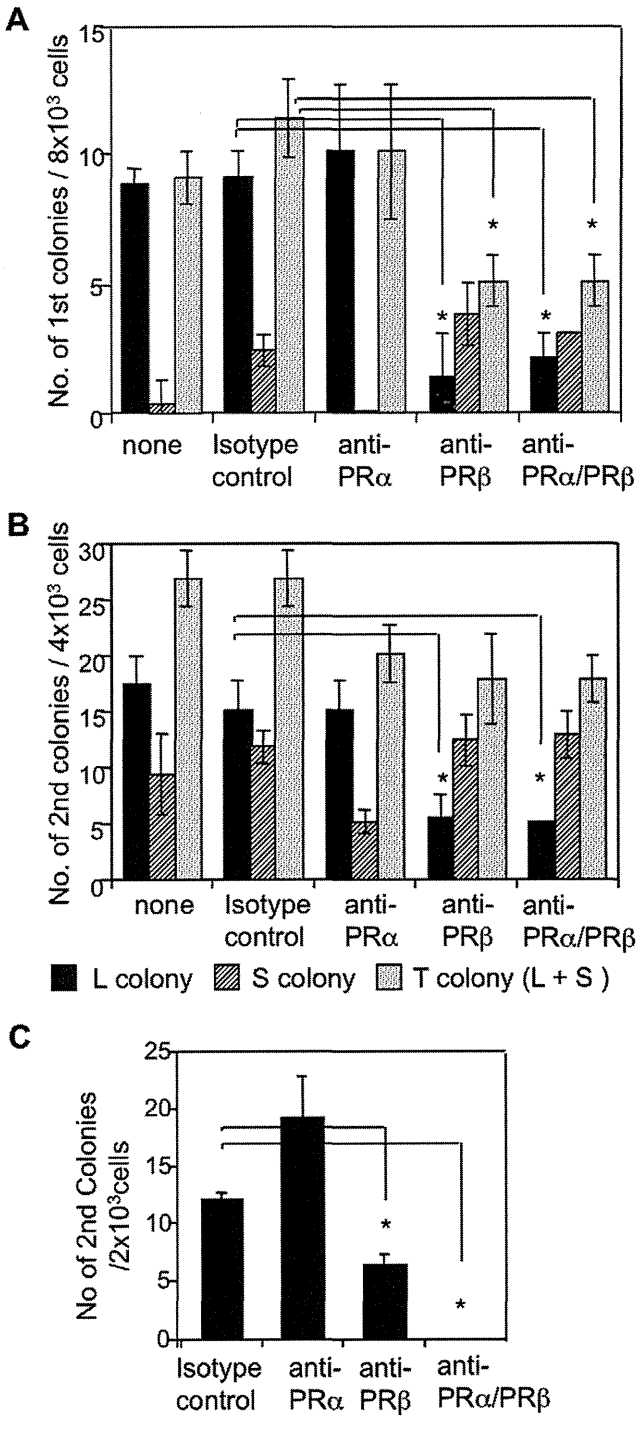

Figure 3. Effects of inhibitory antibodies against PDGFRα and/or PDGFRβ in CFU-F assays using dental mesenchymal cells. (A) Numbers of primary colonies (1st CFU-F) induced from dental mesenchymal cells from 4-week-old mice in the presence of anti-PDGFRα (APA5) and/or anti-PDGFRβ (APB5). None, no antibody. Numbers of large (L, >50 cells), small (clusters) (S, 8–50 cells), and total colonies (T, L+S colonies) are shown. (B) Numbers of secondary colonies (2nd CFU-F) induced from primary colonies of 4-week-old mice in the presence of anti-PDGFRα and/or anti-PDGFRβ. The primary CFU-F assay was performed in the absence of these antibodies. Numbers of large, small, and total colonies are shown. (C) Numbers of secondary colonies (2nd CFU-F) induced from primary colonies from 4,000 dental mesenchymal cells of 4-week-old mice in the presence of anti-PDGFRα and/or anti-PDGFRβ. The secondary CFU-F assay was performed in the

absence of antibodies. Values represent the means (SD) of triplicate cultures. Asterisks indicate a significant difference from the number of colonies in the presence of the isotype-matched control antibody ($p<0.05$). The experiments were repeated twice and one representative experiment is presented.
doi:10.1371/journal.pone.0046436.g003

isotype control in the secondary CFU-F assay (Fig. 3C). Thus, PDGFRβ signaling is important for maintaining self-renewal of dental CFU-Fs, rather than proliferation of CFU-F descendants.

Origins and characteristics of thymic and BM mesenchymal cells

Previously, we reported that multipotent NC-derived cells participate in the formation of fetal thymic and dental mesenchyme [31,32]. However, the origins and characteristics of BM and thymic mesenchymal cells and their MSCs remain unclear. Thus, we examined whether NC-derived and mesoderm-derived cells contributed to BM and thymic mesenchyme from the fetal stage to the adult stage.

In the BM, both Mesp1/YFP$^+$ and P0/YFP$^+$ (Wnt1/YFP$^+$) cells contributed to mesenchyme in E14.5 or E15.5 embryos, two-day-old mice, and adult mice (Fig. 4A, B). However, half of the BM mesenchyme was composed of cells other than P0/YFP$^+$ (Wnt1/YFP$^+$) and Mesp1/YFP$^+$ cells (Fig. 4A–C). Immunohistochemistry detected two-day-old P0/YFP$^+$ and Mesp1/YFP$^+$ BM mesenchymal cells in trabecular and cortical bone (Fig. 4B). Subsequently we reported that fetal thymic and dental mesenchymal cells have the potential to differentiate into melanocytes (a highly reliable marker of NC-derived cells) [31,32]. We confirmed the presence of NC-derived cells in BM, by testing whether these mesenchymal cells differentiate into melanocytes. Pigmented melanocytes were induced from YFP$^+$ cells in BM and YFP$^+$ cells from the skin of E17.5 *P0/YFP* embryos (Fig. 4D). The results suggested that NC-derived cells were present in the BM.

Next, we tested the expression of PDGFRs in BM mesenchymal cells. Unlike dental mesenchyme, PDGFRα- and/or PDGFRβ-expressing cells were present in the YFP$^+$ and YFP$^-$ fractions of BM mesenchymal cells from two-day-old *Mesp1/YFP* and *P0/YFP* mice (Fig. 4 C). The sections showed that two-day-old P0/YFP$^+$ BM mesenchymal cells around the blood vessels expressed α-SMA (Fig. 5A). Furthermore, Mesp1/YFP$^+$ BM mesenchymal cells of the same age expressed CD31 in blood vessels (Fig. 5B). Thus, NC-derived and mesoderm-derived cells in the BM may contribute to α-SMA$^+$ perivascular cells and CD31$^+$ endothelial cells, respectively.

In the thymus, most E13.5 thymic mesenchymal cells (except MHC class II$^+$ thymic epithelial cells) consisted of either Wnt1/YFP$^+$ or Mesp1/YFP$^+$ cells (Fig. 4E), while 86% of CD45$^-$Ter119$^-$ thymic mesenchymal cells from two-day-old mice were composed of either Wnt1/YFP$^+$ cells or Mesp1/YFP$^+$ cells (Fig. 4F). Similar to BM, PDGFRα- and/or PDGFRβ-expressing cells were observed in the YFP$^+$ and YFP$^-$ fractions of thymic mesenchymal cells from two-day-old *Mesp1/YFP* and *Wnt1/YFP* mice (Fig. 4F). The sections indicated that two-day-old Wnt1/YFP$^+$ thymic mesenchymal cells around the blood vessels expressed α-SMA, whereas Mesp1/YFP$^+$ thymic mesenchymal cells of the same age expressed CD31 in blood vessels (Fig. 5C, D). Thus, NC-derived and mesoderm-derived cells in the thymus may contribute to α-SMA$^+$ perivascular cells and CD31$^+$ endothelial cells, respectively.

Origins of BM and thymic CFU-Fs and roles of PDGFRs in these CFU-Fs

The observed discrepancy between PDGFR-expressing cells in the dental mesenchyme, the thymus, and the BM mesenchyme necessitated an assessment of CFU-F origins in the thymus and BM mesenchyme. We performed CFU-F assays using BM mesenchymal cells from two-day-old *Wnt1/YFP* (*P0/YFP*) and *Mesp1/YFP* mice. Unlike the dental mesenchymal cells, Mesp1/YFP$^+$ and Wnt1/YFP$^+$ (P0/YFP$^+$) BM mesenchymal cells exhibited colony-forming capacity (Fig. 6A). Unlike dental and thymic mesenchymal cells, it was unclear whether Mesp1/YFP$^-$ cells were Wnt1/YFP$^+$ (P0/YFP$^+$) NC-derived cells or whether Wnt1/YFP$^-$ (P0/YFP$^-$) cells were Mesp1/YFP$^+$ mesoderm-derived cells, because the mesenchymal cells comprised 1% Wnt1/YFP$^+$, 15% P0/YFP$^+$, and 27% Mesp1/YFP$^+$ cells, indicating that 57% of cells were not Wnt1/YFP$^+$ (P0/YFP$^+$) NC-derived cells or Mesp1/YFP$^+$ mesoderm-derived cells. Therefore, Wnt1/YFP$^-$ (P0/YFP$^-$) and Mesp1/YFP$^-$ mesoderm-derived cells may be present in BM (Figs. 4C, 6A), Nevertheless, Wnt1/YFP$^+$ and P0/YFP$^+$ cells comprised 44% and 85% of BM CFU-Fs, respectively (Fig. 6A, B). P0/YFP$^+$ BM mesenchymal cells from seven-month-old mice continued to exhibit a colony-forming capacity, and cells prepared from these colonies expressed PDGFRα and PDGFRβ (Fig. S4).

A secondary CFU-F assay was performed to investigate the self-renewal activity of BM CFU-Fs. Secondary CFU-Fs in the BM comprised 80% Wnt1/YFP$^+$ and 20% Wnt1/YFP$^-$ cells, or 100% Mesp1/YFP$^-$ cells (Fig. 6C, D). These results suggest that BM MSCs are derived mainly from NC and that they are maintained in older mice.

BM CFU-Fs were present in PDGFRα$^+$ and PDGFRβ$^+$ cells. Because the role of PDGFRs in BM CFU-Fs remained unclear; therefore, we examined the effects of anti-PDGFR antibodies on colony formation. Similar to dental CFU-Fs, the number of CFU-Fs induced from BM cells decreased with the addition of anti-PDGFRα and anti-PDGFRβ to the culture (Fig. 6A, B). The number of YFP$^+$ and YFP$^-$ colonies generated from BM mesenchymal cells of *P0/YFP*, *Wnt1/YFP* and *Mesp1/YFP* mice decreased (Fig. 6A, B). To assess the effects of these antibodies on the self-renewal capacity of CFU-Fs, we performed a primary CFU-F assay with anti-PDGFRβ and anti-PDGFRα antibodies, and a secondary CFU-F assay was performed without either antibody. In the BM mesenchymal cells from *Wnt1/YFP* mice, we found that the number of secondary colonies treated with both antibodies was 40% of that observed in the presence of the isotype control (Fig. 6C). The number of YFP$^+$ secondary colonies induced from the BM of *Wnt1/YFP* and *Mesp1/YFP* mice were reduced in the presence of both antibodies Fig. 6C, D). Irrespective of the origins of cells, it was clear that PDGFRβ signaling was important for maintaining self-renewal of BM CFU-Fs.

Next, we performed CFU-F assays using thymic mesenchymal cells from two-day-old *Wnt1/YFP* and *Mesp1/YFP* mice. Mesp1/YFP$^+$ and Wnt1/YFP$^-$ thymic mesenchymal cells exhibited colony-forming capacity (Fig. 6A). In particular, secondary CFU-Fs in the thymus were derived almost entirely from Mesp1/YFP$^+$ or Wnt1/YFP$^-$ cells (Fig. 6C, D). Similar to the BM CFU-Fs, the number of CFU-Fs induced from thymic cells decreased with the addition of anti-PDGFRα and anti-PDGFRβ to the culture (Fig. 6A, B). The number of YFP$^+$ and YFP$^-$ colonies generated using thymic mesenchymal cells from *Wnt1/YFP* and *Mesp1/YFP* mice decreased (Fig. 6A, B). Furthermore, thymic mesenchymal cells from *Wnt1/YFP* mice and *Mesp1/YFP* mice treated with anti-PDGFRα and anti-PDGFRβ antibody

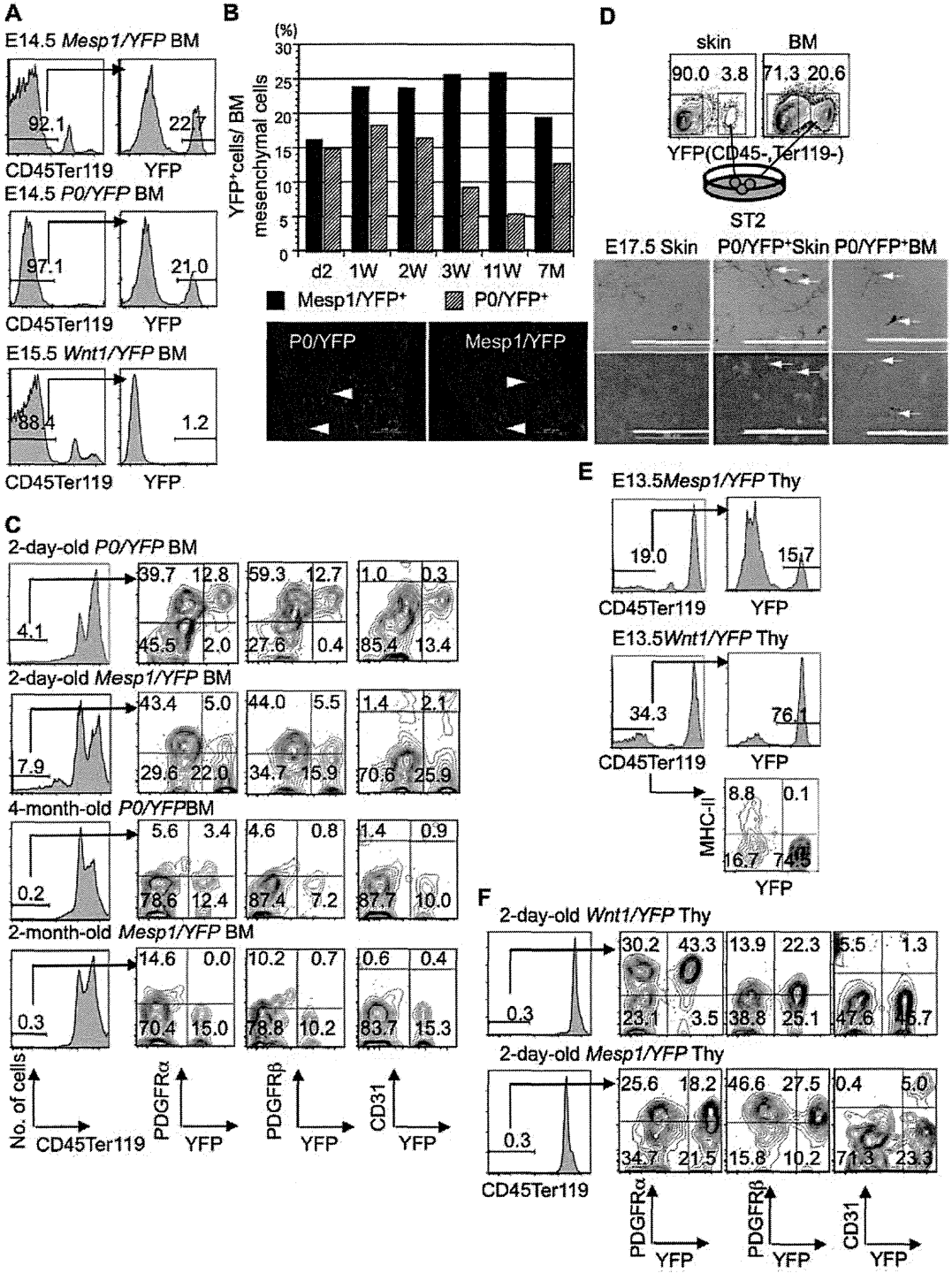

Figure 4. Origins and characteristics of mesenchymal cells in BM and thymus. (A) Contributions of YFP$^+$ mesenchymal cells from *Mesp1-Cre/YFP*, *P0-Cre/YFP*, and *Wnt1-Cre/YFP* embryos to BM. (B) YFP$^+$ cells from BM mesenchyme of *P0-Cre/YFP* and *Mesp1-Cre/YFP* mice from neonatal to adult stages. The mean of two independent experiments is shown. W, week; M, month. Immunohistochemistry for YFP in BM of 2-day-old *P0-Cre/YFP* and *Mesp1-Cre/YFP* mice (lower panel). White arrowheads indicate YFP$^+$ cells in the trabecular and cortical bone. (C) Expression of YFP, PDGFRα, PDGFRβ, and CD31 on BM mesenchymal cells prepared from *P0-Cre/YFP*, *Wnt1-Cre/YFP*, and *Mesp1-Cre/YFP* mice. (D) Induction of melanocytes from the sorted E17.5 P0/YFP$^+$ BM (6.5×10^3). The P0/YFP$^+$ cells from the skin of the same mice (P0/YFP$^+$ skin) and C57BL/6 mice were the controls. White arrows indicate pigmented and YFP$^+$ melanocytes. Scale bars, 200 μm. (E) Contributions of YFP$^+$ mesenchymal cells from *Mesp1-Cre/YFP* and *Wnt1-Cre/YFP* embryos to thymus. (F) Expression of YFP, PDGFRα, PDGFRβ, and CD31 on thymic mesenchymal cells prepared from *Wnt1-Cre/YFP*, and *Mesp1-Cre/YFP* mice. The experiments were repeated and one representative experiment is presented.
doi:10.1371/journal.pone.0046436.g004

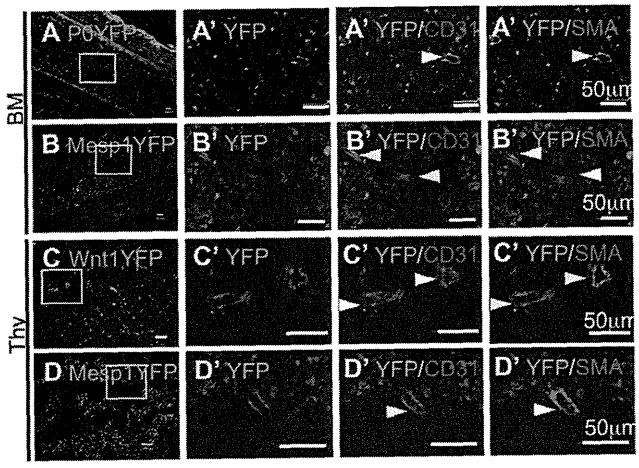

Figure 5. Immunohistochemistry of the BM or thymus of *P0-Cre/YFP*, *Mesp1-Cre/YFP*, and *Wnt1-Cre/YFP* mice. (A–D) Immunohistochemistry for YFP, CD31, and α-SMA in the BM (A, B) or thymus (C, D) of 2-day-old *P0-Cre/YFP* (A), *Mesp1-Cre/YFP* (B, D), and *Wnt1-Cre/YFP* (C) mice. High-magnification views (A'–D') of the boxed areas in (A–D), respectively. Yellow and white arrowheads indicate positive cells for each antibody to indicate the presence or absence of YFP^+ cells, respectively. Scale bars, 50 μm. The experiments were repeated and one representative experiment is presented.
doi:10.1371/journal.pone.0046436.g005

exhibited an unusual capacity for secondary colony formation (Fig. 6C, D). Similar to the BM, PDGFRβ signaling is important for maintaining thymic CFU-Fs containing self-renewal MSCs, irrespective of their origin.

BM and thymic mesenchymal cells can differentiate into osteoblasts, adipocytes, and chondrocytes

We cultured CFU-F progeny to assess the differentiation potential of BM and thymic mesenchymal cells and then found that CFU-F progeny from Wnt1/YFP^+(P0/YFP^+) BM and thymic mesenchymal cells differentiated into osteoblasts, adipocytes, and chondrocytes (Fig. 6E). Unlike dental mesenchymal cells, Mesp1/YFP^+ BM and thymic mesenchymal cells had the potential to differentiate into osteoblasts and adipocytes (Fig. 6E). Thus, CFU-Fs with MSC properties develop mainly from NC and the mesoderm in the BM and thymic mesenchyme.

Dental mesenchymal cells support B lymphopoiesis and osteoclastogenesis

Dental and BM mesenchymal cells have many similarities. BM mesenchymal cells support the differentiation of B lymphocytes and osteoclasts [34,35]. However, it is unclear whether dental mesenchymal cells support the differentiation of these cells. Thus, we prepared dental and BM mesenchymal cells from three-day-old or nine-week-old *Wnt1/YFP* mice. First, we examined the expression of genes encoding the critical hematopoietic factors stem cell factor (SCF), interleukin-7 (IL-7), and CXC chemokine ligand 12 (CXCL12) [36]. Interestingly, dental mesenchyme expresses *Dentin sialophosphoprotein* (*Dspp*, which is an odontoblast-specific gene), *Mgf*, *Il7*, and *Cxcl12*, as does BM mesenchyme (Fig. 7A). To determine whether dental mesenchyme supported the differentiation of B lymphocytes, we prepared dental and BM mesenchymal cells from *Wnt1/YFP* mice. Two weeks later, 200 c-Kit^+ $Sca1^+$ $Lineage^-$ (KSL) cells were isolated from the BM of C57BL/6 mice were cultured in purified YFP^+ dental mesenchyme, which contained 94% YFP^+ cells, and unfractionated BM mesenchymal cells, which contained 18% YFP^+ cells with rmIL-7 (Fig. 7B). Two weeks later, we found that a large number of $CD19^+$ cells (B lineage cells) were induced on Wnt/YFP^+ dental mesenchymal cells (Y^+Tooth), BM mesenchymal cells (unfractionated BM), and ST2 cells, which support the differentiation of B lymphocytes and osteoclasts (Fig. 7B). Next, we studied the possible effects of Wnt/YFP^+ dental mesenchymal cells on osteoclast induction by culturing 100 KSL cells on these mesenchymal cells in the presence of $1\alpha,25(OH)_2D_3$ and Dex. After six days, we induced tartrate-resistant acid phosphatase $(TRAP)^+$ multinucleated osteoclasts on Wnt/YFP^+ dental mesenchymal, BM mesenchymal, and ST2 cells (Fig. 7C). We found that 94% of these dental mesenchymal cells were Wnt/YFP^+ NC-derived cells, which indicated that NC-derived dental mesenchymal cells had similar properties to BM mesenchymal cells in terms of their support of B lymphopoiesis and osteoclastogenesis.

Discussion

This study aimed to investigate the origin and characteristics of dental, thymic, and BM mesenchymal cells and MSCs. We used *Wnt1/YFP* and *P0/YFP* mice as markers of NC-derived cells and *Mesp1/YFP* mice as markers of mesoderm-derived cells. Most dental and thymic mesenchymal cells are composed of Wnt1/YFP^+ NC-derived cells or Mesp1/YFP^+ mesoderm-derived cells (Fig. 8). However, 57% BM mesenchyme comprises cells other than Wnt1/YFP^+ (P0/YFP^+) NC-derived cells or Mesp1/YFP^+ mesoderm-derived cells (Fig. 8). The lateral plate mesoderm (LPM) generates the limb skeleton [37]. Moreover, the *Mesp1* gene is expressed mainly in LPM-derived head mesenchyme and cardiac mesoderm. Therefore, expression of *Mesp1* gene may be insufficient to allow Cre-mediated recombination in LPM, or possibly other mesoderm-derived cells such as the paraxial mesoderm may contribute to LPM. The origin of BM mesenchymal cells may differ from that of dental and thymic mesenchymal cells.

Approximately similar numbers of P0/YFP^+ and Wnt1/YFP^+ cells were observed in the tooth and thymus, whereas larger numbers of P0/YFP^+ cells than Wnt1/YFP^+ cells were detected in BM. Although we cannot explain the difference between the numbers of YFP^+ cells, the fact that YFP^+ BM cells of *P0-Cre/Floxed-EGFP* and *Wnt1-Cre/Floxed-EGFP* mice differentiate into peripheral neurons and glia developing from NC [6], along with our observation that P0/YFP^+ and Wnt1/YFP^+ BM mesenchymal cells differentiate into melanocytes, suggests that *P0/YFP* and *Wnt1/YFP* mice mark NC-derived cells. Because *Wnt1-Cre* is expressed in early migratory NC [5,38], whereas *P0-Cre* is expressed in the early stage of NC cells and in the glial subset of NC cells [30,39], *P0/YFP* may also label other populations of NC-derived cells in addition to the common population of NC-derived cells labeled by both *P0/YFP* and *Wnt1/YFP* mice in BM. Alternatively, the discrepancy between *P0/YFP* and *Wnt1/YFP* mice may be attributed to a Cre-switching efficiency. However, YFP^+ BM mesenchymal cells in *Wnt1/YFP* demonstrated a marked capacity for colony formation, indicating that NC contributes to BM mesenchyme and its MSC. However, ectopic expression of the *P0-Cre* gene occurs in BM cells, because P0/YFP^+ cells were partially detected in hematopoietic cells and marked some non-NC–derived cells, including a minor population of endothelial cells in adult BM [40]. On the other hand, YFP^+ cells in *Sox1-Cre/YFP* mice, which help in tracing neuroepithelial cells, contribute to BM mesenchyme and BM MSCs [7]. The percentage of YFP^+ cells in BM mesenchyme of *Sox1-Cre/YFP*

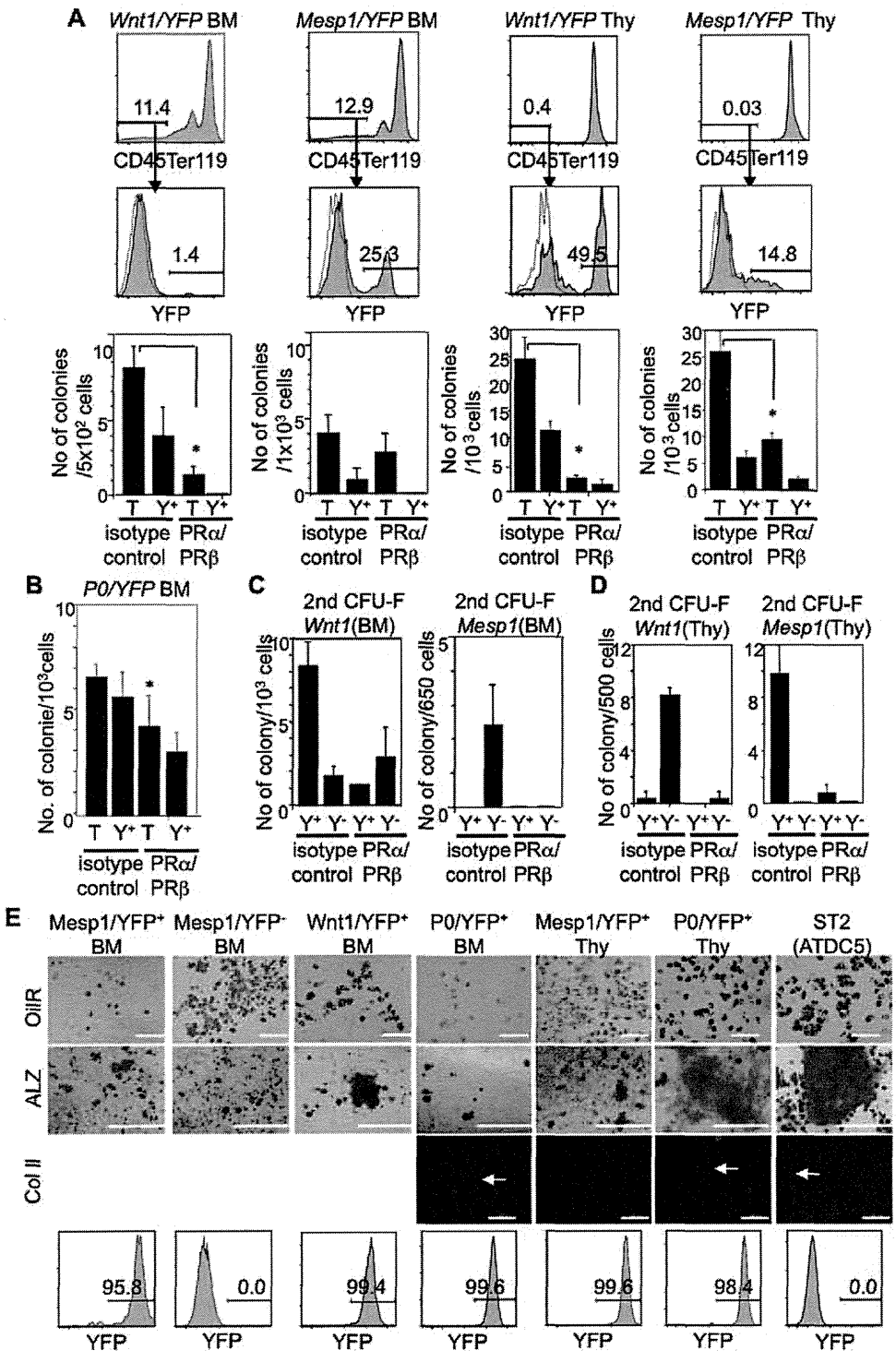

Figure 6. Origins and characteristics of BM and thymic CFU-Fs and roles of PDGFRs in these CFU-Fs. (A) Contributions of YFP$^+$ mesenchymal cells (CD45-Ter119-cells) from 2-day-old *Wnt1-Cre/YFP* and *Mesp1-Cre/YFP* mice to BM and thymus. BM and thymic CFU-F assays were performed in the presence of anti-PDGFRβ (APB5) and anti-PDGFRα (APA5) or isotype-matched control antibody. (B) Numbers of colonies induced from BM mesenchymal cells from 2-day-old *P0-Cre/YFP* mice in the presence of the anti-PDGFRβ and anti-PDGFRα. (C, D) The secondary CFU-F assay using cells from primary colonies induced from 1,000 BM (C) and thymic (D) mesenchymal cells of 2-day-old *Wnt1-Cre/YFP* and *Mesp1-Cre/YFP* mice in the presence of anti-PDGFRα and anti-PDGFRβ antibodies. The secondary CFU-F assay was performed in the absence of antibodies. T, total colonies; Y$^+$, YFP$^+$ colonies; Y$^-$, YFP$^-$ colonies. Values represent the mean (SD) of triplicate cultures. Asterisks indicate a significant difference in the number of colonies compared with that of the isotype-matched control antibody ($p<0.05$). (E) Differentiation potential of thymic and BM mesenchymal cells from *Wnt1-Cre/YFP*, *P0-Cre/YFP*, and *Mesp1-Cre/YFP* mice into adipocytes, osteoblasts, and chondrocytes. YFP expression in each cell preparation is shown in the lower panel. The cultured cells were stained with oil red O (OilR), alizarin red (ALZ), and anti-type II collagen (Col II) antibody to detect adipocytes, osteoblasts, and chondrocytes, respectively. ST2 and ATDC5 cells were the positive controls. The experiments were repeated twice and one representative experiment is presented. Scale bars, 200 μm in OilR and Col II in (E), and 1 mm in (ALZ in E). White arrows indicate positive cells against Col II antibody.

doi:10.1371/journal.pone.0046436.g006

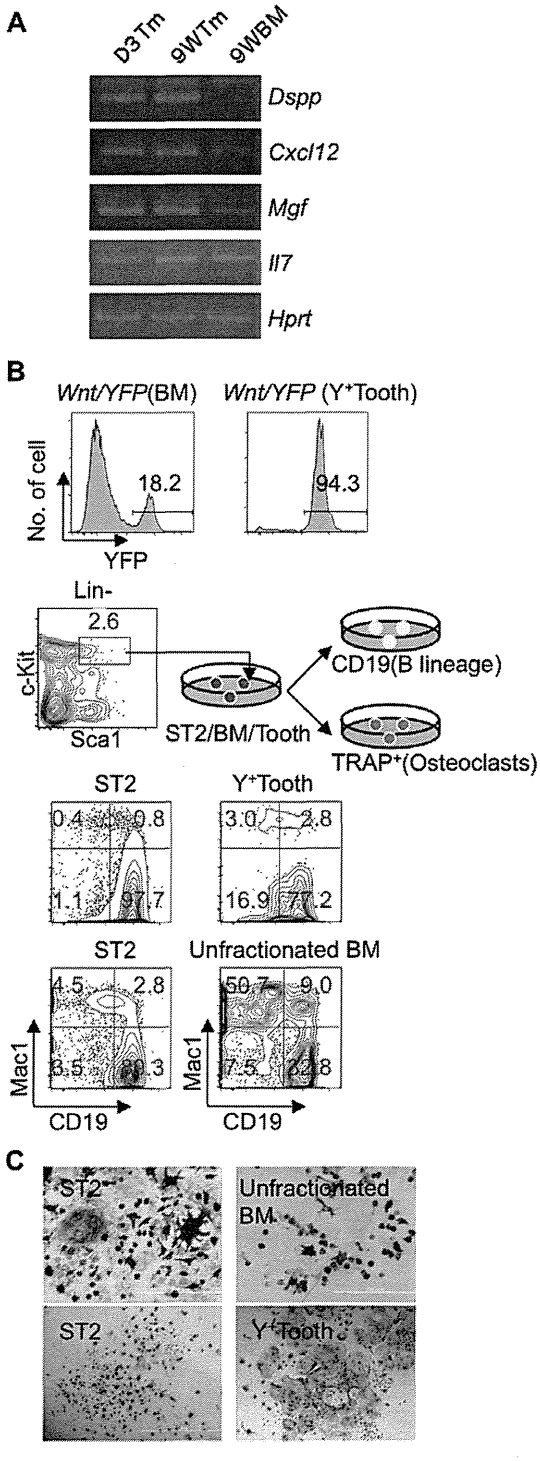

Figure 7. NC-derived dental mesenchymal cells support B lymphopoiesis and osteoclastogenesis. (A) Expression of genes encoding hematopoietic factors on CD45$^-$ and Ter119$^-$ BM mesenchymal cells and dental mesenchymal cells. RT-PCR was performed using RNA from these cells. Hypoxanthine guanidine phosphoribosyl transferase (*Hprt*) was the positive control. D3Tm, dental mesenchymal cells from 3-day-old mice; 9WTm, dental mesenchymal cells from 9-week-old mice; 9WBM, CD45$^-$ and Ter119$^-$ BM mesenchymal cells from 9-week-old mice. (B) Induction of B lineage cells. Unfractionated BM and purified YFP$^+$ dental mesenchymal cells (Y$^+$ Tooth) from 3-day-old *Wnt1-Cre/YFP* mice were cultured. Percentages of YFP$^+$ cells in the CD45$^-$ and Ter119$^-$ fractions after 2 weeks' culture (upper panels). BM-derived 200 KSL cells were then cultured on purified YFP$^+$ dental mesenchymal cells (Y$^+$ Tooth) or unfractionated BM mesenchymal cells in the presence of rmIL-7. Mac1 and CD19 were used as Myeloid cell lineage and B cell lineage markers. (C) Osteoclast induction. One hundred KSL cells were cultured on unfractionated BM and YFP$^+$ dental mesenchymal cells (Y$^+$ Tooth) prepared from the same mice in the presence of $1\alpha,25(OH)_2D_3$, and DEX. TRAP staining was performed to detect osteoclasts. ST2 stromal cells were used as the positive control to support the differentiation of B lymphocytes and osteoclasts. Each experiment with BM or dental mesenchyme is shown with ST2 as the control (B, C). Each experiment was repeated twice and one representative experiment is presented. Scale bars, 200 μm.
doi:10.1371/journal.pone.0046436.g007

mice was almost similar to that of YFP$^+$ cells from *Wnt1/YFP* mice.

The origins of dental pulp stem cells and stem cells from human exfoliated deciduous teeth (SHEDs) are unclear [16,19]. Because odontoblasts generally develop from NC, SHEDs that can differentiate into odontoblasts, osteoblasts, and neurons may develop from NC-derived cells. Contrary to our results, Iohara et al. reported that side population (SP) cells of adult porcine dental mesenchymal cells can differentiate into odontoblasts, chondrocytes, adipocytes, neurons, and endothelial cells [41]. These multipotent SP cells express CD31, CD34, FLK1, and CD105 (endothelial markers), but scarcely express α-SMA or NG2 (perivascular cell markers). Because endothelial cells are of mesodermal origin [42], these SP cells may be more immature than NC-derived cells or may comprise both NC-derived and mesoderm-derived cells.

Wnt1/YFP$^+$, unlike Mesp1/YFP$^+$ dental mesenchymal cells, exhibited marked potential for colony formation in the CFU-F assays. Because dental pulp includes small numbers of Mesp1/YFP$^+$ mesoderm-derived cells, we calculated the ratio of the number of YFP$^+$ colonies to the total number of YFP$^+$ mesenchymal cells in the CFU-F assays. The frequency of CFU-Fs within YFP$^+$ dental mesenchymal cells was lower than 1/2,040 (1/1,080) and 1/1,178 (1/728) in E13 (2-day-old) *Mesp1/YFP* and *Wnt1/YFP* mice, respectively. Mesp1/YFP$^+$ dental mesenchymal cells may rarely possess colony-forming capacity in the CFU-F assays. Although Mesp1/YFP$^+$ thymic and BM mesenchymal cells differentiate into adipocytes and osteoblasts, Mesp1/YFP$^+$ dental mesenchymal cells rarely differentiate into osteoblasts and chondrocytes *in vitro*, even when they successfully proliferate. Mesp1/YFP$^+$ mesoderm-derived cells in the dental mesenchyme may already have lost the potential to differentiate into osteoblasts and chondrocytes or be committed to endothelial cells.

Human dental pulp stem cells or SHEDs are similar to BM MSCs with regard to the expression of cell-surface antigens such as STRO1$^+$ and α-SMA$^+$ (perivascular cell markers) and CD146$^+$ (a perivascular cell and endothelial cell marker) [43]. In mouse dental pulp and BM cells, PDGFR-expressing cells have shown colony-forming capacity *in vitro*. However, unlike dental CFU-Fs, BM and thymic CFU-Fs comprise both Wnt1/YFP$^+$ (P0/YFP$^+$) NC-derived cells and Mesp1/YFP$^+$ mesoderm-derived cells. Furthermore, self-renewing CFU-Fs, including MSCs, consist entirely of Wnt1/YFP$^+$ (P0/YFP$^+$) NC-derived cells in the teeth, and mostly Wnt1/YFP$^+$ (P0/YFP$^+$) NC-derived cells in BM. We also showed that NC-derived dental mesenchymal cells expressed genes encoding critical hematopoietic factors such as IL-7, SCF, and CXCL12, and they supported the differentiation of B lymphocytes and osteoclasts [36,44]. Although it is unclear whether NC-derived and/or mesoderm-derived BM mesenchymal cells support B lymphopoiesis and osteoclasts, it is well known that cotransplantation of BM mesenchymal cells with hematopoietic cells promotes the reconstitution of hematopoiesis [45]. Because dental mesenchymal cells facilitate the easy preparation of MSCs compared

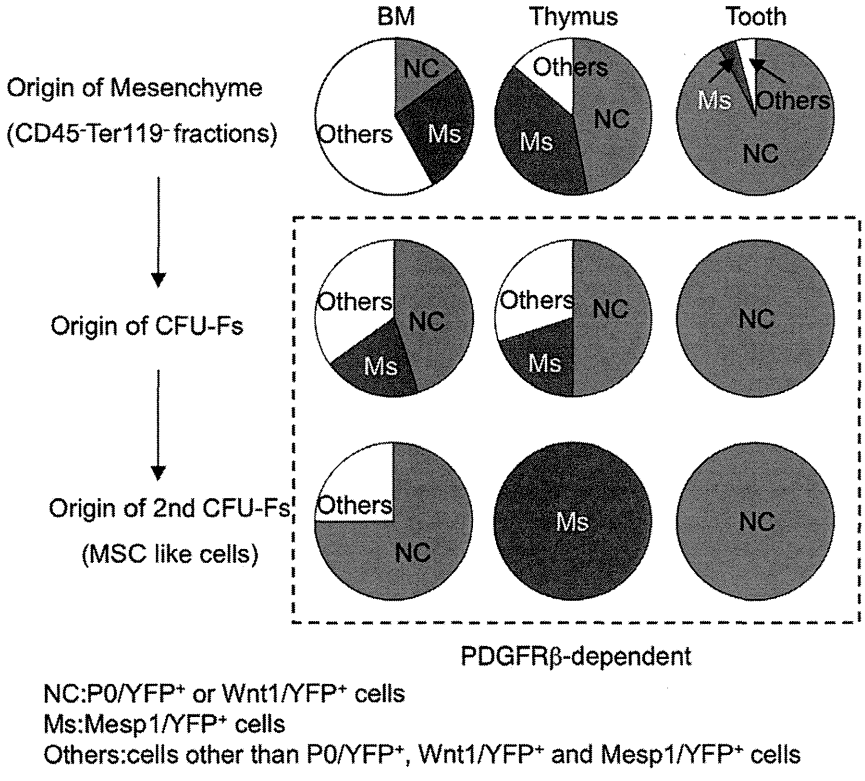

Figure 8. Origin and properties of dental, thymic, and BM mesenchymal cells and their CFU-Fs. Percentages of NC-derived and mesoderm-derived cells comprising BM, thymic, and dental mesenchyme (CD45$^-$ and Ter119$^-$ cells). YFP$^+$ cells in CD45$^-$ and Ter119$^-$ cells from *P0-Cre/YFP* and *Wnt1-Cre/YFP* mice represent NC-derived cells (NC). YFP$^+$ cells in CD45$^-$ and Ter119$^-$ cells from *Mesp1-Cre/YFP* mice represent mesoderm-derived cells (Ms). YFP$^-$ cells other than YFP$^+$ cells in the CD45$^-$ and Ter119$^-$ cells from *P0-Cre/YFP* (*Wnt1-Cre/YFP*) and *Mesp1-Cre/YFP* mice represent others. The expression of primary and secondary CFU-Fs *in vitro* was dramatically affected by PDGFRβ inhibition, irrespective of tissue and origin.
doi:10.1371/journal.pone.0046436.g008

with BM stromal cells, dental mesenchyme may represent a useful resource in improving hematopoiesis in patients with hematopoietic disorders. However, it is still not clear the role of NC-derived cells or mesoderm-derived cells in the BM and thymic lympho-hematopoiesis. Further examination is desire to elucidate these roles.

We first indicated that an inhibitory antibody against PDGFRβ decreased the CFU-F count. Retention of 15% CFU-Fs generated in the control culture in the presence of anti-PDGFRβ implies that both PDGFRβ-dependent and PDGFRβ-independent CFU-Fs are present in the dental pulp, BM, and thymus. Simultaneous addition of anti-PDGFRα and anti-PDGFRβ more effectively blocked secondary colony formation in dental and thymic CFU-F progeny. Because PDGFRα is upregulated in response to *Pdgfrb* mutation [46], anti-PDGFRβ–treated cells may increase PDGFRα expression and become sensitive to anti-PDGFRα.

Conclusion

This is the first report to demonstrate that both NC-derived and mesoderm-derived cells with CFU-F capacity contribute to the dental pulp, thymus, and BM from the fetal stage to the adult stage. Although the origin of self-renewing CFU-Fs differs by tissue, these CFU-Fs are dependent on PDGFRβ irrespective of their origin.

Materials and Methods

Animals and Ethics Statement

P0-Cre, *Wnt1-Cre*, and *Rosa26EYFP* mice were provided by Drs. K. Yamamura (Kumamoto University), H. Sucov (Southern California University), and H. Enomoto (RIKEN Kobe), respectively [47]. *Mesp1-Cre* and C57BL/6 mice were obtained from the Riken Bioresource Center and Clea Japan, Inc., respectively. All mice were maintained at the Institute of Laboratory Animals, Mie University; all experimental procedures were approved by the Institutional Animal Care and Use Committee of Mie University (approval number 20–22), and were performed according to the Mie University guidelines for laboratory animals.

Preparation of single-cell suspensions

The mandibular molar tooth buds and dental pulp of the lower incisors were incubated with 2.4 U dispase II (Roche) in 10% FBS/HBSS for 30 min at 4°C and 1 mg/mL collagenase D (Roche) in 10% FBS/HBSS for 2 h at 37°C. Thymi were incubated with 1 mg/mL collagenase D in 10% FBS/HBSS for 1 h at 37°C. Femora and tibia were minced and were incubated with 2.0 U dispase II and 0.1 mg/mL collagenase D in 10% FBS/HBSS for 1 h at 37°C, and then in 2% FBS/HBSS for 1 h at 37°C. The dorsal regions of E9.5 embryos were dissected and incubated with 2.4 U dispase II in 10% FBS/HBSS at 4°C for 1 h, minced, and then incubated with 1 mg/mL collagenase D in

10% FBS/HBSS for 1 h at 37°C. Pipetted single-cell suspensions were used for further procedures.

RNA isolation and RT-PCR

Total RNA was prepared using Trizol (Invitrogen). cDNA synthesis was carried out using reverse transcriptase (ReverTraAce; Toyobo) and oligo (dT) primers (Toyobo). PCR using cDNA was performed with r*Taq* polymerase (Toyobo) and the forward primers and reverse primers were as follows: *AP2*: 5′-AGGGACTTTGGGTACGTGTG-3′, 5′-AGGGCCTGGGTGAGATAGTT-3′; *p75(NGFR)*: 5′-TGCTGCTGCTGCTGCTGCTTCT-3′, 5′-CGGGTCCACGTGGTTGGCTTCATCT-3′; *Sox10*: 5′-CACTACACCGACCAGCCGTCCACTT-3′, 5′-GATAGAGTCGTATATACTGGCTGCT-3′; *Krox20*: 5′-ACCCCTGGATCTCCCGTATCCGAGT-3′, 5′-GGACAGGGAAACGGCTTTCGATCTG-3′; *Brachyury(T)*: 5′-CTCCAACCTATGCGGACAAT-3′, 5′-CCCCTTCATACATCGGAGAA-3′; *Dentin sialophosphoprotein(Dspp)*: 5′-ACATTGTTGAAAACTCTGTGGCTGTGCCTC-3′, 5′-CATTTGCTGTGCTGTTCTCTCCTCTCGCAT-3′; *Il7*: 5′-ACATCATCTGAGTGCCACA-3′, 5′-CTCTCAGTAGTCTCTTTAG-3′; *Mgf*: 5′-GTGGCAAATCTTCCAAATGA-3′, 5′-CTCGGGACCTAATGTTGAAG-3′; *Cxcl12*: 5′-GCTCTGCATCAGTGACGGTAAAC-3′, 5′-GCAATATCGTACCATATGCTATGGC-3′; *Hprt*: 5′-AGTTCTTTGCTGACCTGCTG-3′, 5′-GCTTTGTATTGGGCTTTTCC-3′. PCR was performed as follows: 94°C for 4 min; 35 cycles at 93°C for 1 min, 55°C (*Mgf*, *Cxcl12*), 56°C (*Il7*), 58°C (*Sox10*, *Dspp*, *Hprt*), 60°C (*AP2*, *Krox20*, *Brachyury*), 63°C (*p75*) for 1 min, and 72°C for 1 min; and extension at 72°C for 7 min.

Antibodies

The following antibodies were used: biotin-conjugated PDGFRβ (APB5; eBioscience); Pacific Blue-conjugated streptavidin (eBioscience); APC-conjugated PDGFRα (APA5; eBioscience), PDGFRβ (APB5), CD31 (PECAM1) (MEC13.3; eBioscience), Mac1 (M1/70; Biolegend), and c-Kit (2B8; eBioscience); Cy7PE-conjugated CD45 (30-F11; eBioscience), Ter119 (eBioscience), and CD19 (6D5; Biolegend); Pacific Blue-conjugated Sca1 (Ly-6 A/E) (E13-161.7; Biolegend); PE-conjugated MHC Class II (I-Ab) (25-9-17; BD Pharmingen), FLK1 (Avasα1; eBioscience), and CD34 (RAM34; BD Pharmingen); rabbit anti-mouse p75NGFR polyclonal antibody (Chemicon); Alexafluor 405-conjugated goat anti-rabbit IgG (Invitrogen); biotin-conjugated CD4 (GK1.5; eBioscience), CD8α (53-6.7; eBioscience), Mac1 (M1/70), Gr1 (RB6-8C5; eBioscience), B220 (6B2; eBioscience), and Ter119; and PE-conjugated streptavidin.

Cell sorting and analysis

Cells were analyzed on FACS Aria or FACS Canto II (BD), followed by analyses with FlowJo software (Tree Star).

Immunohistochemistry

Molar tooth germs, lower incisors, thymi, and femora were fixed in 4% paraformaldehyde and embedded in cryomold for sectioning (10 μm). The following antibodies were used: Alexafluor 488-conjugated rabbit anti-GFP IgG (Invitrogen), rat anti-mouse CD31 (PECAM-1) (MEC13.3), DyLight™ 649-conjugated AffiniPure donkey anti-rat IgG (H+L) (Jackson ImmunoResearch Laboratory), Cy3-conjugated mouse anti–α-smooth muscle actin (α-SMA) (1A4) (Sigma), mouse anti–neuron-specific β-tubulin III (TUJ1; Babco), and Cy3-conjugated AffiniPure donkey anti-mouse polyclonal IgG (HL) (Jackson ImmunoResearch Laboratory). Images were captured using confocal microscopy (Olympus FV1000D).

CFU-F assays

Mesenchymal cells from tooth buds, dental pulp, BM, and thymi of *P0-Cre/YFP*, *Wnt1-Cre/YFP*, and *Mesp1-Cre/YFP* mice were cultured in α-MEM with 20% FBS in 6-well plates in the presence/absence of inhibitory antibodies against PDGFRα (anti-PDGFRα, APA5) [48] and/or PDGFRβ (anti-PDGFRβ, APB5) [49]; antibodies against c-Kit (ACK4) and IL-7Rα (A7R) were used as isotype-matched controls in BM and thymic cultures, respectively. Inhibitory antibodies against c-Fms (AFS98) were used to inhibit macrophage proliferation. Two weeks later, large (>50 cells) and small colonies (clusters <50 cells) and YFP^+ and YFP^- colonies were scored as primary CFU-Fs [17]. For secondary CFU-F assays to detect self-renewing CFU-Fs, cells from primary colonies were cultured in the presence/absence of antibodies. Selected YFP^+/YFP^- primary colonies were cultured to establish YFP^+ clones.

Induction of adipocytes, osteoblasts, and chondrocytes

For osteoblast induction, 100,000 cells were cultured in DMEM medium (Gibco) supplemented with 10% FBS, 10^{-7} M Dexamethasone (DEX; Sigma), 40 nM human ascorbic acid 2 phosphatase (Sigma), 1 nM BMP4 (Neomarker), and 10 mM β-glycerophosphate (Sigma) [32,50]. For adipocyte induction, 100,000 cells were cultured in α-MEM supplemented with 10% FBS, 0.25 μM DEX, 0.5 mM 3-isobutyl-1-methylxanthine (Sigma), 1 μM Triiodo (Sigma), and 0.2 μ M insulin (Sigma) [51]. For chondrocyte induction, 200,000 cells (1×10^7/mL) were cultured in α-MEM supplemented with 10% FBS, 10^{-7} M DEX, 40 nM ascorbic acid-2-phosphatase, and 1 nM TGFβ3 or BMP2 (Neomarker) [49]. After 2–3 weeks, cells were stained with oil red-O (OilR), alizarin red (ALZ), and mouse anti-type II collagen antibody (6B3, Neomarker) and Cy3-conjugated goat anti-mouse IgG (Jackson ImmunoResearch Laboratory) to detect adipocytes, osteoblasts, and chondrocytes, respectively. ST2 and ATDC5 cells were the positive controls for osteogenesis and adipogenesis, and chondrogenesis, respectively [52].

Induction of B lymphocytes and osteoclasts

Dental and BM mesenchymal cells were prepared from 3-day-old *Wnt1-Cre/YFP* mice. Femoral c-Kit^+ $Sca1^+$ $Lineage^-$ (KSL) cells were isolated from 8-week-old C57BL/6 mice. For B lymphocyte induction, 200 KSL cells were cultured on purified YFP^+ dental mesenchymal cells or unfractionated BM mesenchymal cells in RPMI-1640 (Gibco) supplemented with 10% FBS, 5×10^{-5} M 2ME, and 10 ng/mL rmIL-7 (Invitrogen). After 2 weeks, cells collected were analyzed by FACS. For osteoclast induction, 100 KSL cells were cultured on these mesenchymal cells in α-MEM supplemented 10% FBS, 10^{-7} M DEX, and 10^{-7} M 1α, 25-dihydroxyvitamin D ($1\alpha,25(OH)_2D_3$) (Biomol Research Laboratory). After 6 days, TRAP activity of cells was studied to detect osteoclasts [34]. ST2 cells were the positive control used for the differentiation of B lymphocytes and osteoclasts [34,35].

Induction of melanocytes from BM mesenchymal cells

Single-cell suspensions from BM of *P0-Cre/YFP* embryos were prepared. Sorted YFP^+ BM mesenchymal cells from *P0-Cre/YFP* embryos (20,000) were cultured on ST2 cells in α-MEM containing 10% FBS with 10^{-7} M DEX, 20 pM rhbFGF (R&D Systems), 10 pM cholera toxin (Sigma), and 40 nM rhET3

(Peptide Institute) [31]. Skin YFP$^+$ cells of the same mice were used as a positive control. The pigmented melanocytes were microscopically examined after 3 weeks.

Statistical analysis

Data are expressed as means (SD). Statistical significance was assessed using Student's *t*-test.

Supporting Information

Figure S1 Expression of NC- and mesoderm-associated genes on cells from *P0-Cre/YFP*, *Wnt1-Cre/YFP*, and *Mesp1-Cre/YFP* mice. (A) Expression of p75NGFR on cells in the CD45$^-$ and Ter119$^-$ fractions from E9.5 *P0-Cre/YFP* and *Wnt1-Cre/YFP* embryos. Empty means secondary antibody only (Alexafluor 405-conjugated goat anti-rabbit IgG) without primary antibody. (B) Expression of NC-associated genes on cells from E9.5 *P0-Cre/YFP*, *Wnt1-Cre/YFP*, and *Mesp1-Cre/YFP* embryos ($n=4$/group). (C) Expression of NC- and mesoderm-associated genes in dental mesenchymal cells from *Wnt1-Cre/YFP* mice ($n=4$/group). YFP$^+$ and YFP$^-$ cells were isolated using a cell sorter. RT-PCR was performed using RNA from these cells. Hypoxanthine guanidine phosphoribosyl transferase (*Hprt*) was the positive control; no expression was detected without a template (data not shown).
(TIF)

Figure S2 Expression of cell-surface antigens related to endothelial cells on dental mesenchymal cells from 4-week-old *Wnt1-Cre/YFP* and *Mesp1-Cre/YFP* mice. Expression of cell-surface antigens related to endothelial cells on YFP$^+$ or YFP$^-$ dental mesenchymal cells in CD45$^-$ and Ter119$^-$ fractions from 4-week-old *Wnt1-Cre/YFP* and *Mesp1-Cre/YFP* mice. The experiments were repeated twice and one representative experiment is presented.
(TIF)

Figure S3 Expression of PDGFR and CD31 on dental mesenchymal cells from CFU-F progenies of 4-week-old *Mesp1-Cre/YFP* or *Wnt1-Cre/YFP* mice. (A) Number of colonies in the tertiary CFU-F assay using YFP$^-$ and YFP$^+$ dental mesenchymal cells isolated from secondary CFU-F progenies from *Mesp1-Cre/YFP* mice. Values represent the mean (SD) of triplicate cultures. (B) Expression of PDGFRa and PDGFRβ on YFP$^-$ and YFP$^+$ dental mesenchymal cells from secondary CFU-F progenies from *Mesp1-Cre/YFP* mice. (C) Expression of CD31 and PDGFRβ on YFP$^+$ and YFP$^-$ cells recovered from primary CFU-F progenies from *Mesp1-Cre/YFP* and *Wnt1-Cre/YFP* mice. The experiments were repeated twice and one representative experiment is presented.
(TIF)

Figure S4 CFU-Fs of BM mesenchymal cells from 7-month-old *P0-Cre/YFP* mice. (A) Numbers of colonies induced from BM mesenchymal cells from 7-month-old *P0-Cre/YFP* mice. (B) Expression of YFP, PDGFRα, and PDGFRβ on cells from these colonies. Values represent the mean (SD) of triplicate cultures. The experiments were repeated twice and one representative experiment is presented.
(TIF)

Table S1 The number of primary and secondary colonies and the origin of colony-forming cells in dental mesenchymal cells. Numbers of primary colonies (1st CFU-F, >50 cells) induced from 4×10^3 dental mesenchymal cells from 4-week-old *Wnt1-Cre/YFP* and *Mesp1-Cre/YFP* mice. Numbers of secondary colonies (2nd CFU-F, >50 cells) induced from 1×10^3 primary colonies of 4-week-old mice. Values represent the means (SD) of triplicate cultures. Asterisks indicate total number of colonies obtained from triplicate cultures of two independent experiments.
(DOC)

Table S2 Effects of inhibitory antibodies against PDGFRs in CFU-F assays using dental mesenchymal cells. Numbers of colonies were induced from 8×10^3 dental mesenchymal cells prepared from 4-week-old *Wnt1-Cre/YFP* mice in the presence of inhibitory antibody against PDGFRα (APA5) and/or inhibitory antibody against PDGFRβ (APB5). No add means no antibody, and control means isotype-matched control antibody (ACK4). All antibodies were used in 10 mg/ml. Numbers of large (L, >50 cells), small (clusters) (S, <50 cells), and total colonies (T, L+S colonies) are shown. Values represent the means (SD) of triplicate cultures. Asterisks indicate a significant difference from the number of colonies in the presence of the isotype-matched control antibody ($p<0.05$). The experiments were repeated twice and one representative experiment is presented.
(DOC)

Acknowledgments

We thank Drs. S. Iseki and T. Shigeoka for their helpful discussion; Drs. K. Yamamura, H. Sucov, and H. Enomoto for providing the *P0-Cre*, *Wnt1-Cre*, and *Rosa26EYFP* mice; Dr. S. Nishikawa for providing the monoclonal antibodies (ACK4, A7R, and AFS98); and Ms. Yamada for technical assistance. The authors would like to thank Enago (www.enago.jp) for the English language review.

Author Contributions

Conceived and designed the experiments: HY TY. Performed the experiments: YK DK KI HY. Analyzed the data: HY TY. Contributed reagents/materials/analysis tools: NT. Wrote the paper: HY TY SH.

References

1. Anderson DJ (1997) Cellular and molecular biology of neural crest cell lineage determination. Trends Genet 13: 276–280.
2. Le Douarin NM, Kalcheim C (1999) Cell lineage segregation during neural crest ontogeny. The Neural Crest. In: Le Douarin NM, Kalcheim, C eds. Cambridge: Cambridge University Press. pp. 304–335.
3. Bockman DE, Kirby ML (1984) Dependence of thymus development on derivatives of the neural crest. Science 223: 498–500.
4. Le Douarin NM, Jotereau FV (1975) Tracing of cells of the avian thymus through embryonic life in interspecific chimeras. J Exp Med 142:17–40.
5. Jiang X, Rowitch DH, Soriano P, McMahon AP, Sucov HM (2000) Fate of the mammalian cardiac neural crest. Development 127: 1607–1616.
6. Nagoshi N, Shibata S, Kubota Y, Nakamura M, Nagai Y, et al. (2008) Ontogeny and multipotency of neural crest-derived stem cells in mouse bone marrow, dorsal root ganglia, and whisker pad. Cell Stem Cell 2: 392–403.
7. Takashima Y, Era T, Nakao K, Kondo S, Kasuga M, et al. (2007) Neuroepithelial cells supply an initial transient wave of MSC differentiation. Cell 129: 1377–1388.
8. Etchevers HC, Vincent C, Le Douarin NM, Couly GF (2001) The cephalic neural crest provides pericytes and smooth muscle cells to all blood vessels of the face and forebrain. Development 128: 1059–1068.
9. Yoshida T, Vivatbutsiri P, Morriss-Kay G, Saga Y, Iseki S (2008) Cell lineage in mammalian craniofacial mesenchyme. Mech Dev 125: 797–808.
10. Foster K, Sheridan J, Veiga-Fernandes H, Roderick K, Pachnis V, et al. (2008) Contribution of neural crest-derived cells in the embryonic and adult thymus. J Immunol 180: 3183–3189.
11. Chung UI, Kawaguchi H, Takato T, Nakamura K (2004) Distinct osteogenic mechanisms of bones of distinct origins. J Orthop Sci 9: 410–414.
12. Couly GF, Coltey PM, Le Douarin NM (1993) The triple origin of skull in higher vertebrates: a study in quail-chick chimeras. Development: 117: 409–429.

13. Harel I, Nathan E, Tirosh-Finkel L (2009) Distinct origins and genetic programs of head muscle satellite cells. Dev Cell 16: 822–832.
14. McBratney-Owen B, Iseki S, Bamforth SD, Olsen BR, Morriss-Kay GM (2008) Development and tissue origins of the mammalian cranial base. Dev Biol: 322: 121–132.
15. Matsuoka T, Ahlberg PE, Kessaris N, Iannarelli P, Dennehy U, et al. (2005) Neural crest origins of the neck and shoulder. Nature 436: 347–355.
16. Gronthos S, Mankani M, Brahim J, Robey PG, Shi S (2000) Postnatal human dental pulp stem cells (DPSCs) in vitro and in vivo. Proc Natl Acad Sci U S A 97: 13625–13630.
17. Friedenstein AJ, Chailakhjan RK, Lalykina KS (1970) The development of fibroblast colonies in monolayer cultures of guinea-pig bone marrow and spleen cells. Cell Tissue Kinet 13: 393–403.
18. Jiang Y, Jahagirdar BN, Reinhardt RL, Schwartz RE, Keene CD, et al. (2002) Pluripotency of mesenchymal stem cells derived from adult marrow. Nature 418: 41–49.
19. Miura M, Gronthos S, Zhao M, Lu B, Fisher LW, et al. (2003) SHED: stem cells from human exfoliated deciduous teeth. Proc Natl Acad Sci U S A 100: 5807–5812.
20. Pittenger MF, Mackay AM, Beck SC, Jaiswal RK, Douglas R, et al. (1999) Multilineage potential of adult human mesenchymal stem cells. Science 284: 143–147.
21. Kruger GM, Mosher JT, Bixby S, Joseph N, Iwashita T, et al. (2002) Neural crest stem cells persist in the adult gut but undergo changes in self-renewal, neuronal subtype potential, and factor responsiveness. Neuron 35: 657–669.
22. Morikawa S, Mabuchi Y, Kubota Y, Nagai Y, Niibe K, et al. (2009) Prospective identification, isolation, and systemic transplantation of multipotent mesenchymal stem cells in murine bone marrow. J Exp Med 206: 2483–2496.
23. Morrison SJ, White PM, Zock C, Anderson DJ (1999) Prospective identification, isolation by flow cytometry, and in vivo self-renewal of multipotent mammalian neural crest stem cells. Cell 96: 737–749.
24. Morikawa S, Mabuchi Y, Niibe K, Suzuki S, Nagoshi N, et al. (2009) Development of mesenchymal stem cells partially originate from the neural crest. Biochem Biophys Res Commun 379: 1114–1119.
25. Sieber-Blum M, Grim M, Hu YF, Szeder V (2004) Pluripotent neural crest stem cells in the adult hair follicle. Dev Dyn 231: 258–269.
26. Wong CE, Paratore C, Dours-Zimmermann MT, Rochat A, Pietri T, et al. (2006) Neural crest-derived cells with stem cell features can be traced back to multiple lineages in the adult skin. J Cell Biol 175:1005–1015.
27. Chai Y, Jiang X, Ito Y, Bringas P Jr, Han J, et al. (2000) Fate of mammalian cranial neural crest during tooth and mandibular morphogenesis. Development 127: 1671–1679.
28. Saga Y, Miyagawa-Tomita S, Takagi A, Kitajima S, Miyazaki J, et al. (1999) MesP1 is expressed in the heart precursor cells and required for the formation of a single heart tube. Development 126: 3437–3447.
29. Soriano P (1999) Generalized lacZ expression with the ROSA26 Cre reporter strain. Nat Genet 21: 70–71.
30. Yamauchi Y, Abe K, Mantani A, Hitoshi Y, Suzuki M, et al. (1999) A novel transgenic technique that allows specific marking of the neural crest cell lineage in mice. Dev Biol 212: 191–203.
31. Yamazaki H, Sakata E, Yamane T, Yanagisawa A, Abe K, et al. (2005) Presence and distribution of neural crest-derived cells in the murine developing thymus and their potential for differentiation. Int Immunol 17: 549–558.
32. Yamazaki H, Tsuneto M, Yoshino M, Yamamura K, Hayashi S (2007) Potential of dental mesenchymal cells in developing teeth. Stem Cells 25: 78–87.
33. Gronthos S, Simmons PJ (1995) The growth factor requirements of STRO-1-positive human bone marrow stromal precursors under serum-deprived conditions in vitro. Blood 85(4): 929–940.
34. Yamazaki H, Kunisada T, Yamane T, Hayashi S (2001) Presence of osteoclast precursors in colonies cloned in the presence of hematopoietic colony-stimulating factors. Exp Hematol 29: 68–76.
35. Nishikawa S, Ogawa M, Nishikawa S, Kunisada T, Kodama H (1988) B lymphopoiesis on stromal cell clone: stromal cell clones acting on different stages of B cell differentiation. Eur J Immunol 18: 1767–1771.
36. Tagaya H, Kunisada T, Yamazaki H, Yamane T, Tokuhisa T, et al. (2000) Intramedullary and extramedullary B lymphopoiesis in osteopetrotic mice. Blood 95(11): 3363–3370.
37. Gilbert SF (2010) Chapter 11, Paraxial mesoderm and intermediate mesoderm. Developmental Biology, 9th Edition. In: Carol Wigg ed. Sinauer Associates Inc. pp. 413–444.
38. Echelard Y, Vassileva G, McMahon AP (1994) Cis-acting regulatory sequences governing Wnt-1 expression in the developing mouse CNS. Development 120(8): 2213–2224.
39. Messing A, Behringer RR, Hammang JP, Palmiter RD, Brinster RL, et al. (1992) P0 promoter directs expression of reporter and toxin genes to Schwann cells of transgenic mice. Neuron 8(3): 507–520.
40. Kubota Y, Takubo K, Hirashima M, Nagoshi N, Kishi K, et al. (2011) Isolation and function of mouse tissue resident vascular precursors marked by myelin protein zero. J Exp Med 208(5): 949–960.
41. Iohara K, Zheng L, Ito M, Tomokiyo A, Matsushita K, et al. (2006) Side population cells isolated from porcine dental pulp tissue with self-renewal and multipotency for dentinogenesis, chondrogenesis, adipogenesis, and neurogenesis. Stem Cells 24: 2493–2503.
42. Hirashima M, Kataoka H, Nishikawa S, Matsuyoshi N, Nishikawa S (1999) Maturation of embryonic stem cells into endothelial cells in an in vitro model of vasculogenesis. Blood 93: 1253–1263.
43. Shi S, Gronthos S (2003) Perivascular niche of postnatal mesenchymal stem cells in human bone marrow and dental pulp. J Bone Miner Res 18: 696–704.
44. Sugiyama T, Kohara H, Noda M, Nagasawa T (2006) Maintenance of the hematopoietic stem cell pool by CXCL12-CXCR4 chemokine signaling in bone marrow stromal cell niches. Immunity 25(6): 977–988.
45. Bensidhoum M, Chapel A, Francois S, Demarquay C, Mazurier C, et al. (2004) Homing of in vitro expanded Stro-1− or Stro-1+ human mesenchymal stem cells into the NOD/SCID mouse and their role in supporting human CD34 cell engraftment. Blood 103(9): 3313–3319.
46. Soriano P (1994) Abnormal kidney development and hematological disorders in PDGF beta-receptor mutant mice. Genes Dev 8:1888–1896.
47. Srinivas S, Watanabe T, Lin CS, William CM, Tanabe Y, et al. (2001) Cre reporter strains produced by targeted insertion of EYFP and ECFP into the ROSA26 locus. BMC Dev Biol 1, 4
48. Takakura N, Yoshida H, Ogura Y, Kataoka N, Nishikawa S, et al. (1997) PDGFR alpha expression during mouse embryogenesis: immunolocalization analyzed by whole-mount immunohistostaining using the monoclonal anti-mouse PDGFR alpha antibody APA5. J Histochem Cytochem 45: 883–893.
49. Sano H, Sudo T, Yokode M, Murayama T, Kataoka N, et al. (2001) Functional blockade of platelet-derived growth factor receptor-beta but not of receptor-alpha prevents vascular smooth muscle cell accumulation in fibrous cap lesions in apolipoprotein E-deficient mice. Circulation 103: 2955–2960.
50. Kramer J, Hegert C, Rohwedel J (2003) In vitro differentiation of mouse ES cells: bone and cartilage. Methods Enzymol 365: 251–268.
51. Dani C, Smith AG, Dessolin S, Leroy P, Staccini L, et al. (1997) Differentiation of embryonic stem cells into adipocytes in vitro. J Cell Sci 110: 1279–1285.
52. Atsumi T, Miwa Y, Kimata K, Ikawa Y (1990) A chondrogenic cell line derived from a differentiating culture of AT805 teratocarcinoma cells. Cell Differ Dev 30: 109–116.

Immunity
Article

The Transcription Factor Jdp2 Controls Bone Homeostasis and Antibacterial Immunity by Regulating Osteoclast and Neutrophil Differentiation

Kenta Maruyama,[1] Masahiro Fukasaka,[1] Alexis Vandenbon,[2] Tatsuya Saitoh,[1] Takumi Kawasaki,[1] Takeshi Kondo,[1] Kazunari K. Yokoyama,[4] Hiroyasu Kidoya,[3] Nobuyuki Takakura,[3] Daron Standley,[2] Osamu Takeuchi,[1,5] and Shizuo Akira[1,3,*]

[1]Laboratory of Host Defense
[2]Laboratoy of Systems Immunology, WPI Immunology Frontier Research Center (IFReC)
[3]Research Institute for Microbial Diseases
Osaka University, Osaka 565-0871, Japan
[4]Cancer Center, Kaohsiung Medical University Hospital, 807 Kaohsiung, Taiwan
[5]Laboratory of Infection and Prevention, Institute for Virus Research, Kyoto University, Kyoto 606-8507, Japan
*Correspondence: sakira@biken.osaka-u.ac.jp
http://dx.doi.org/10.1016/j.immuni.2012.08.022

SUMMARY

Jdp2 is an AP-1 family transcription factor that regulates the epigenetic status of histones. Previous in vitro studies revealed that Jdp2 is involved in osteoclastogenesis. However, the roles of Jdp2 in vivo and its pleiotropic functions are largely unknown. Here we generated *Jdp2*$^{-/-}$ mice and discovered its crucial roles not only in bone metabolism but also in differentiation of neutrophils. *Jdp2*$^{-/-}$ mice exhibited osteopetrosis resulting from impaired osteoclastogenesis. *Jdp2*$^{-/-}$ neutrophils were morphologically normal but had impaired surface expression of Ly6G, bactericidal function, and apoptosis. We also found that ATF3 was an inhibitor of neutrophil differentiation and that Jdp2 directly suppresses its expression via inhibition of histone acetylation. Strikingly, *Jdp2*$^{-/-}$ mice were highly susceptible to *Staphylococcus aureus* and *Candida albicans* infection. Thus, Jdp2 plays pivotal roles in in vivo bone homeostasis and host defense by regulating osteoclast and neutrophil differentiation.

INTRODUCTION

Jun dimerization protein 2 (Jdp2) is a member of the AP-1 family and interacts with other AP-1 components, such as c-Jun, JunB, JunD, and ATF2 (Aronheim et al., 1997). Jdp2 can inhibit the activation of its binding partners, suggesting that it is a transcriptional repressor (Jin et al., 2001). Furthermore, Jdp2 suppresses histone acetyltransferase activity and acetylation of reconstituted nucleosomes, thereby regulating the epigenetic status of histones (Jin et al., 2006). Extensive studies have revealed that Jdp2 plays roles in various cellular responses, such as UV-induced apoptosis and osteoclastogenesis (Huang et al., 2010).

Osteoclasts are multinucleated cells that degrade bone (Karsenty and Wagner, 2002). Bone-forming osteoblasts express macrophage colony-stimulating factor (M-CSF) and RANK ligand (RANKL). When these cytokines stimulate their receptors, c-fms and RANK, respectively, transcription factors such as c-Fos, NF-κB, and NFATc1 (Takayanagi, 2007) are activated in osteoclast precursors and osteoclastogenesis is induced by stimulation of osteoclastogenic genes, such as tartrate-resistant acid phosphatase (TRAP) and cathepsin K (CTSK). Jdp2 was previously implicated in positive regulation of osteoclastogenesis via activation of the TRAP and CTSK promoters (Kawaida et al., 2003). Recent findings indicate that the Jdp2 locus is hypomethylated and that its transcript is upregulated in common myeloid precursors and granulocyte-macrophage progenitors relative to lymphoid lineages (Ji et al., 2010), suggesting that Jdp2 may also contribute to the differentiation of myeloid cells, such as neutrophils.

Neutrophils are critical for bacterial clearance. One of the most impressive morphological features of mature neutrophils is cytosolic granules, and the mRNA expressions of granule content genes are significantly higher in immature neutrophils than in mature neutrophils (Borregaard and Cowland, 1997; Borregaard et al., 2007). There are three different granule subtypes, i.e., primary, secondary, and tertiary, and the granule proteins play pivotal roles in bacterial killing. The other bactericidal agents derived from neutrophils are reactive oxygen species (ROS), such as superoxide (Forman and Thomas, 1986). Recently, a novel mechanism of bacterial and fungal killing mediated by chromatin structures was elucidated, termed the neutrophil extracellular trap (NET) (Brinkmann et al., 2004). This extracellular structure is released through a cell death requiring ROS production (Nishinaka et al., 2011) and chromatin decondensation (Li et al., 2010). Collectively, these findings demonstrate that neutrophils exert bactericidal activity through several complex machineries.

Generally, neutrophil subtypes can be distinguished by their surface markers CD11b and Ly6G. CD11b^{+}Ly6G^{lo} cells are immature neutrophils with a round nucleus, such as myelocytes, whereas CD11b^{+}Ly6G^{hi} cells are band-segmented mature neutrophils (Hestdal et al., 1991). By using such morphological and molecular cues, several studies have shown that various cytokines and transcription factors are critical for proper

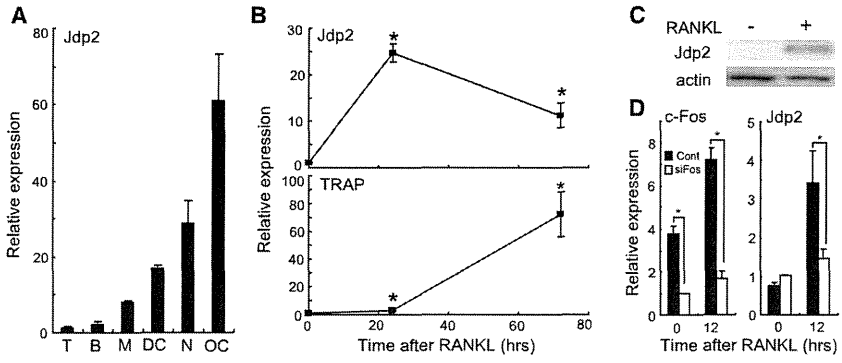

Figure 1. Jdp2 Expression

(A) qPCR analysis of Jdp2 in splenic T cells (T), B cells (B), DCs (DC), neutrophils (N), and primary bone marrow osteoclasts (OC) (n = 3).

(B) qPCR analysis of Jdp2 in MDMs in response to RANKL stimulation. *p < 0.05 versus 0 hr (n = 3).

(C) MDMs were stimulated with 50 ng/ml RANKL for 30 hr. Jdp2 levels were analyzed by protein immunoblotting.

(D) MDMs were transfected with control siRNA (Cont) or c-Fos-specific siRNA (siFos) and stimulated with 50 ng/ml RANKL for 12 hr. c-Fos and Jdp2 levels were measured by qPCR (n = 3).

*p < 0.05 versus control siRNA. Error bars, SE.

development of neutrophils. For example, granulocyte colony-stimulating factor (G-CSF) plays a pivotal role in proliferation of neutrophil precursors via activation of STAT3 (Lieschke et al., 1994). The CCAAT/enhancer binding protein (C/EBP) family is also critically involved in neutrophil differentiation. In particular, C/EBPα is considered a master regulator of neutrophils because C/EBPα-deficient mice lack neutrophils (Zhang et al., 1998). C/EBPε is involved in proper neutrophil differentiation, because neutrophils from C/EBPε-deficient mice have abnormal respiratory burst activity and lack secondary and tertiary granules (Yamanaka et al., 1997). Recent reports have also implicated the transcription factors Gfi-1 (Hock et al., 2003) and Ikaros (Dumortier et al., 2003) in proper differentiation of neutrophils. Overall, these findings suggest that neutrophil differentiation is orchestrated by interplay among several transcription factors.

Despite its importance in in vitro osteoclastogenesis and several implications for its activity in myeloid lineage cells, the roles of Jdp2 in vivo and its pleiotropic functions are completely unknown. Here, we generated *Jdp2*$^{-/-}$ mice and discovered critical roles of Jdp2 not only in bone homeostasis but also in proper differentiation of neutrophils.

RESULTS

Jdp2$^{-/-}$ Mice Are Osteopetrotic because of Impaired Osteoclastogenesis

First, we examined Jdp2 expression in mature myeloid cells, such as macrophages, dendritic cells (DCs), neutrophils, and osteoclasts. Jdp2 expression was substantially higher in these cells than in lymphoid cells, such as T and B cells (Figure 1A). Because Jdp2 expression was highest in osteoclasts (Figure 1A), we focused on the regulation of Jdp2 expression in response to RANKL. Jdp2 expression was significantly increased in M-CSF-derived macrophages (MDMs) after RANKL stimulation (Figures 1B and 1C) but not after LPS stimulation (Figure S1 available online). This transcriptional induction was dependent on c-Fos (based on siRNA knockdown), which is recognized as a pivotal transcription factor for osteoclastogenesis (Figure 1D). The existence of this c-Fos-Jdp2 axis prompted us to explore the role of Jdp2 in RANKL-induced osteoclastogenesis.

To evaluate osteoclastogenesis in vitro, *Jdp2*$^{-/-}$ mice were generated (Figures S2A–S2C). Surprisingly, in vitro RANKL-induced osteoclastogenesis and resorption pit formation were completely abrogated in *Jdp2*$^{-/-}$ cells (Figure 2A). We also evaluated the characteristics of splenic macrophages and found that the populations were similar between wild-type and *Jdp2*$^{-/-}$ cells (Figures S2D, S2E, and S2G). In addition, *Jdp2*$^{-/-}$ MDMs exhibited normal proliferation (Figure S2F) and RANK and c-fms expression (Figure S2H).

As previously reported (Kawaida et al., 2003), induction of osteoclast-associated genes, including TRAP and CTSK, was abrogated in *Jdp2*$^{-/-}$ cells, whereas c-Fos induction was comparable between wild-type and *Jdp2*$^{-/-}$ cells (Figure 2B). We also found that induction of NFATc1 mRNA and DNA binding of NFATc1 to its promoter was partially suppressed in *Jdp2*$^{-/-}$ cells in response to RANKL (Figures S2I and S2J). In addition, Jdp2 had no effect on NFATc1 binding to its promoter region (Figure S2K). Furthermore, DNA binding of NF-κB p65 was normal (Figure S2L). The expression levels of Blimp1, a positive regulator of osteoclastogenesis (Nishikawa et al., 2010), and Blimp1 target genes, such as *Irf8* and *Bcl6*, were comparable (Figure S2M). RANKL-induced calcium oscillation was normal in *Jdp2*$^{-/-}$ cells (Figure S2N). Because TREM2 is required for osteoclast multinucleation (Humphrey et al., 2006), we examined the TREM2 expression levels in wild-type and *Jdp2*$^{-/-}$ MDMs but found no difference (Figure S2O). When TREM2 was stimulated by antibody, wild-type MDMs formed increased numbers of osteoclasts. In contrast, TREM2 stimulation had no effect on osteoclastogenesis of *Jdp2*$^{-/-}$ MDMs (Figures S2P and S2Q). Finally, retrovirus reconstitution of Jdp2 in *Jdp2*$^{-/-}$ MDMs rescued RANKL-induced osteoclastogenesis (Figures S2R and S2S). Together, these results indicate that the c-Fos-Jdp2 axis is critical for controlling osteoclastogenesis via proper induction of NFATc1 and osteoclastogenic genes, such as *TRAP* and *CTSK*.

These findings prompted us to explore the role of Jdp2 in in vivo bone homeostasis. No apparent abnormalities were observed in *Jdp2*$^{-/-}$ mice, although they did exhibit slightly shortened femurs (Figure 2D). Radiographic analysis of the femurs showed that *Jdp2*$^{-/-}$ mice had osteopetrosis accompanied by marked increases in trabecular bone volume and number, compared with wild-type mice (Figures 2C, 2F, and 2G). These findings were further supported by increased bone mineral density (BMD) in the full-length femurs of *Jdp2*$^{-/-}$ mice (Figure 2E). Sections of proximal tibias from *Jdp2*$^{-/-}$ mice also showed increased trabecular bone volume and number (Figures 2H and 2I). Histomorphometric analysis revealed

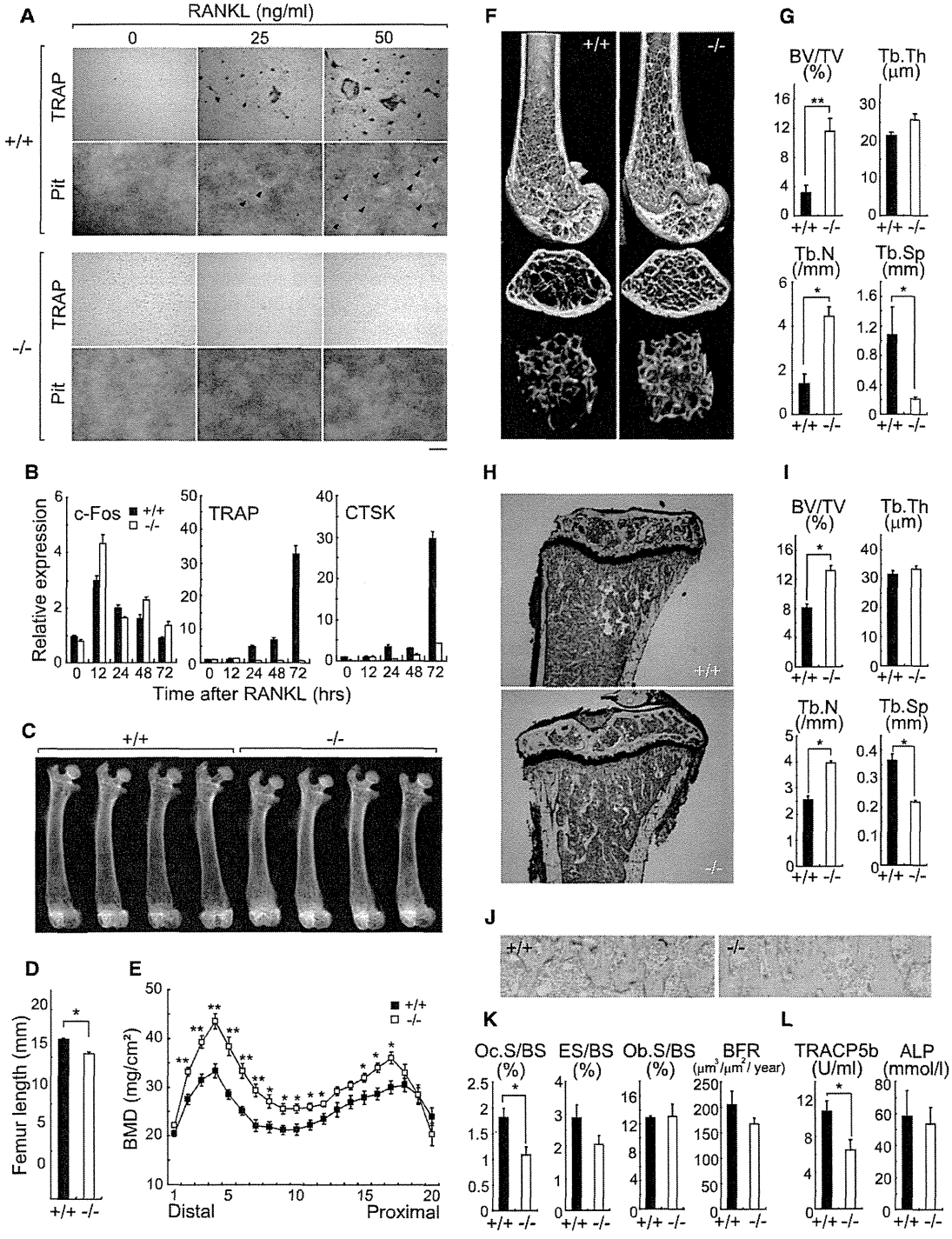

Figure 2. Impaired Osteoclastogenesis in *Jdp2*$^{-/-}$ Mice

(A) MDMs from wild-type and *Jdp2*$^{-/-}$ mice were cultured with the indicated concentrations of RANKL. Representative TRAP staining and resorption pits (*arrowheads*) are shown. Scale bar represents 200 μm.

(B) qPCR analysis of c-Fos, TRAP, and CTSK in wild-type and *Jdp2*$^{-/-}$ MDMs stimulated with 50 ng/ml RANKL (n = 3).

(C) Soft X-ray images of femurs.

(D) Femur lengths.

(E) BMDs of 20 longitudinal femur divisions.

(F) Representative μCT images of distal femurs (top, longitudinal view; middle, axial view of metaphyseal region; bottom, 3D view of metaphyseal region).

(G) Bone morphometric analysis of distal femurs by μCT.

a significant reduction in the osteoclast surface/bone surface ratio in *Jdp2*$^{-/-}$ mice, whereas the osteoblast surface/bone surface ratio and bone formation rate were normal (Figures 2J and 2K). Consistent with the decreased osteoclastogenesis in vivo, the serum bone resorption marker TRACP5b was lower in *Jdp2*$^{-/-}$ mice (Figure 2L). Furthermore, wild-type mice engrafted with bone marrow cells from *Jdp2*$^{-/-}$ mice had an increased bone volume phenotype (Figures S2T and S2U). Collectively, these results indicate that Jdp2 is critical for controlling osteoclastogenesis both in vitro and in vivo.

Neutrophils in *Jdp2*$^{-/-}$ Mice Are Morphologically Normal but Show Impaired Ly6G Expression

A recent report suggested that Jdp2 may be involved in the choice between lymphoid or myeloid differentiation (Ji et al., 2010). Therefore, we focused on the populations of lymphoid and myeloid cells (Figure S3A). No differences in the expressions of cell surface phenotype markers and numbers and ratios of T cells, B cells, and DCs in the spleen were observed between wild-type and *Jdp2*$^{-/-}$ mice (Figure S3A). We also checked the cytokine production (Figures S3B and S3C), bactericidal function (Figure S3D), superoxide production (Figure S3E), and phagocytosis activity (Figure S3F) in *Jdp2*$^{-/-}$ MDMs and conventional DCs (cDCs), and all phenotypes were normal.

Because Jdp2 was highly expressed in mature splenic neutrophils (Figure 1A), we compared the Jdp2 mRNA and protein expression between splenic and bone marrow neutrophils. Jdp2 expression in bone marrow mature CD11b^{+}Ly6G^{hi} neutrophils was lower than that in splenic mature CD11b^{+}Ly6G^{hi} neutrophils, but higher than that in bone marrow immature CD11b^{+}Ly6G^{lo} neutrophils (Figures S3G and S3H). These findings suggest that Jdp2 gradually increases during neutrophil differentiation and maturation.

To check the maturity of neutrophils from *Jdp2*$^{-/-}$ mice, we performed FACS analyses by using CD11b and Ly6G markers (Figure 3A). In *Jdp2*$^{-/-}$ bone marrow cells, the proportion of the CD11b^{+}Ly6G^{hi} population was shifted toward the CD11b^{+} Ly6G^{lo} population (Figure 3A). This low level of Ly6G indicated accumulation of immature cells. However, contrary to our expectation, *Jdp2*$^{-/-}$ neutrophils displayed a normal segmented nuclear morphology (Figure 3A). Because the CD11b^{+} population includes a Ly6C^{hi}Ly6G^{lo} inflammatory monocyte population (Colonna et al., 2004; Lagasse and Weissman, 1996) and a Ly6C^{lo}Ly6G^{+} neutrophil population, CD11b^{+} cells were further gated on CD11b^{+}Ly6C^{lo}Ly6G^{+} neutrophils and CD11b^{+}Ly6C^{hi} Ly6G^{lo} inflammatory monocytes to exclude monocytes from the *Jdp2*$^{-/-}$ CD11b^{+}Ly6G^{+} population (Figure 3B). Among CD11b^{+}Ly6C^{lo}Ly6G^{+} neutrophil populations, the CD11b^{+}Ly6C^{lo} Ly6G^{hi} population was shifted to the CD11b^{+}Ly6C^{lo}Ly6G^{lo} population in *Jdp2*$^{-/-}$ mice (Figure 3B). In contrast, CD11b^{+} Ly6C^{hi}Ly6G^{lo} inflammatory monocyte populations were comparable between wild-type and *Jdp2*$^{-/-}$ cells (Figure 3B). We also confirmed that both wild-type and *Jdp2*$^{-/-}$ CD11b^{+}Ly6C^{lo}Ly6G^{+} neutrophil populations had similar segmented nuclei (Figure 3B).

To further assess the abnormal bone marrow CD11b^{+} Ly6C^{lo}Ly6G^{+} neutrophil population in *Jdp2*$^{-/-}$ mice, we analyzed the cellular microstructure by transmission electron microscopy (TEM) (Figure 3C). However, the intracellular morphology of *Jdp2*$^{-/-}$ cells seemed normal (Figure 3C). To determine whether the abnormal neutrophils accumulated only in the bone marrow, we performed FACS analyses of thioglycollate-elicited peritoneal neutrophils and splenocytes (Figures 3D and 3E). An atypical CD11b^{+}Ly6C^{lo}Ly6G^{lo} population was observed in *Jdp2*$^{-/-}$ peritoneal (Figure 3D) and splenic (Figure 3E) neutrophils. To determine whether the defect in neutrophils in *Jdp2*$^{-/-}$ mice was bone marrow derived and cell intrinsic, we engrafted irradiated wild-type mice with *Jdp2*$^{-/-}$ or wild-type bone marrow. After reconstitution, we observed the same phenotype of neutrophils in the wild-type mice with *Jdp2*$^{-/-}$ bone marrow as in the *Jdp2*$^{-/-}$ mice (Figures S3O–S3Q). Together, these findings suggest that *Jdp2*$^{-/-}$ neutrophils are morphologically normal but have diminished Ly6G expression and that this abnormality arises in a cell-intrinsic manner.

Impaired Apoptosis and Bactericidal Function in *Jdp2*$^{-/-}$ Neutrophils

Intriguingly, we observed slight increases in CD11b^{+}Ly6C^{lo} Ly6G^{+} neutrophil numbers (~20%) in *Jdp2*$^{-/-}$ bone marrow and peripheral populations (Figures 3A, 3B, and 3E). Given this observation, we examined the spontaneous apoptosis of *Jdp2*$^{-/-}$ peritoneal neutrophils (Figure 3F). To our surprise, *Jdp2*$^{-/-}$ neutrophils showed impaired apoptosis compared with wild-type neutrophils (Figure 3F). Microarray and quantitative PCR (qPCR) analyses of neutrophils revealed that Bcl-2 expression was significantly increased in *Jdp2*$^{-/-}$ neutrophils, whereas Jdp2 deficiency had no effect on the diverse array of other Bcl-2-associated genes (Figures 3G–3I). Next, several assays were used to examine *Jdp2*$^{-/-}$ peritoneal neutrophil function. First, the capacity of *Jdp2*$^{-/-}$ mice to recruit neutrophils into the peritoneal cavity after thioglycollate injection was determined, with no difference in cell numbers found between wild-type and *Jdp2*$^{-/-}$ mice (Figure S3I). Second, we checked the cytokine production by *Jdp2*$^{-/-}$ neutrophils and found that Jdp2 deficiency did not alter cytokine production in response to TLR ligands (Figure S3J). Third, we analyzed the function of Jdp2 in NET formation. Intriguingly, we observed a 50% reduction in NET formation in neutrophils from *Jdp2*$^{-/-}$ mice in response to *Staphylococcus aureus* and *Candida albicans* infection (Figures 3J–3M). Fourth, because ROS, such as superoxide, are required for NET formation, we quantified superoxide production by *Jdp2*$^{-/-}$ neutrophils in

(H) Representative proximal tibias.
(I) Bone morphometric analysis of proximal tibias.
(J) TRAP staining of metaphyseal portions of tibias.
(K) Bone histomorphometric analysis of metaphyseal portions of tibias.
(L) Serum levels of TRACP5b and alkaline phosphatase (ALP).
Abbreviations: BV/TV, bone volume per tissue volume; Tb.Th, trabecular bone thickness; Tb.N, trabecular bone number; Tb.Sp, trabecular bone spacing; Oc.S/BS, osteoclast surface per bone surface; ES/BS, eroded surface per bone surface; Ob.S/BS, osteoblast surface per bone surface; BFR, bone formation rate. Error bars, SE. *$p < 0.05$; **$p < 0.01$ ($n = 4$).

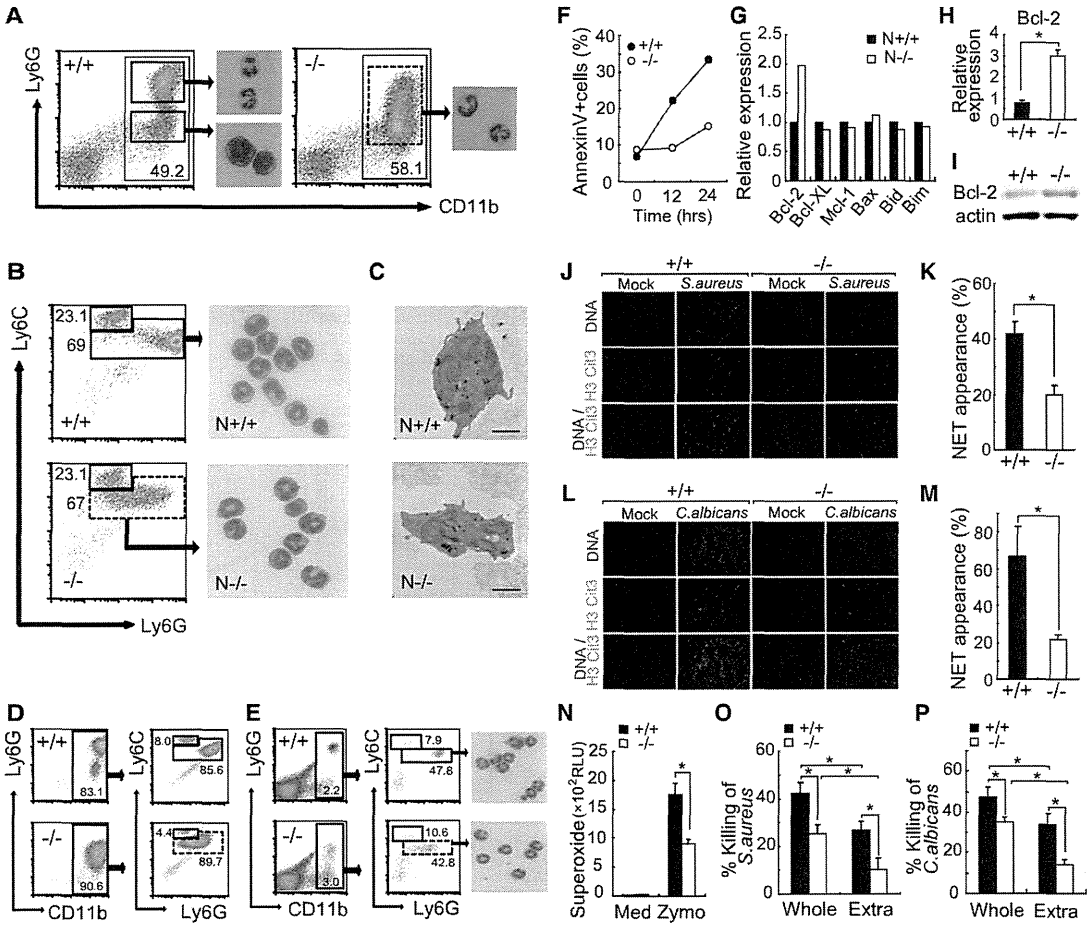

Figure 3. Abnormal Phenotype of *Jdp2*$^{-/-}$ Neutrophils

(A) FACS analysis of wild-type and *Jdp2*$^{-/-}$ bone marrow cells via Ly6G and CD11b markers. Gated cells were sorted and stained with May-Grunwald-Giemsa.

(B) CD11b^{+} populations in (A) were further analyzed with Ly6C marker. CD11b^{+}Ly6C^{lo}Ly6G^{+} neutrophils (N+/+ and N−/−) were sorted and stained as in (A).

(C) N+/+ and N−/− cells were fixed, stained with diaminobenzidine, and analyzed by TEM. Scale bars represent 2 μm.

(D and E) Peritoneal neutrophils (D) and splenocytes (E) were analyzed as in (B).

(F) Peritoneal neutrophils were cultured in vitro and analyzed for the percentage of annexin V-positive cells by FACS (n = 3 independent experiments).

(G) mRNA levels of apoptosis-regulating genes in bone marrow CD11b^{+}Ly6C^{lo}Ly6G^{+} neutrophils (N+/+ and N−/−) analyzed by a microarray.

(H and I) Bcl2 mRNA (H) and protein (I) expression levels in wild-type and *Jdp2*$^{-/-}$ peritoneal neutrophils were analyzed by qPCR and protein immunoblotting, respectively (n = 3).

(J) Peritoneal neutrophils were infected by *S. aureus* for 2 hr (MOI = 50) and stained by Hoechst and anti-histone H3 Cit3 Ab. DNA-histone H3 Cit3 Ab double-positive structures were defined as NETs.

(K) 50 microscopic fields (40×) in wells containing *S. aureus*-infected neutrophils, shown in (J), were checked and the rate of NET appearance was calculated (n = 4 observations).

(L) Peritoneal neutrophils were infected by *C. albicans* for 2 hr (MOI = 50) and stained as in (J).

(M) *C. albicans*-induced NET formation in (L) was measured as in (K).

(N) Peritoneal neutrophils were stimulated with 100 μg/ml Zymosan for 15 min and supernatant superoxide levels were measured.

(O) *S. aureus* killing by peritoneal neutrophils. Phagocytosis was inhibited by cytochalasin D and bacterial killing was measured (Extra) (n = 6).

(P) *C. albicans* killing by peritoneal neutrophils was determined as in (O).

Error bars, SE. *p < 0.05.

response to Zymosan and Curdlan. We observed 50% reductions in superoxide production in *Jdp2*$^{-/-}$ neutrophils (Figures 3N and S3L). We also checked the expression of Dectin-1, a Curdlan receptor, and observed similar expression levels between wild-type and *Jdp2*$^{-/-}$ neutrophils (Figure S3K). To clarify the mechanisms of decreased superoxide production in Jdp2 deficiency, we checked the expression levels of NADPH oxidase subunits and found that NCF1 expression was lower in *Jdp2*$^{-/-}$ neutrophils than in wild-type cells (Figure S3M). Therefore, we infected *Jdp2*$^{-/-}$ neutrophils with a retrovirus encoding NCF1 and measured the superoxide production. However, the rescue of *Jdp2*$^{-/-}$ neutrophils by NCF1 was less efficient than that by Jdp2 (Figure S3N). Thus, increased NCF1 can partially rescue the impaired superoxide production in *Jdp2*$^{-/-}$ neutrophils. Finally, to determine whether the functional defects of *Jdp2*$^{-/-}$ neutrophils were associated with bacterial killing

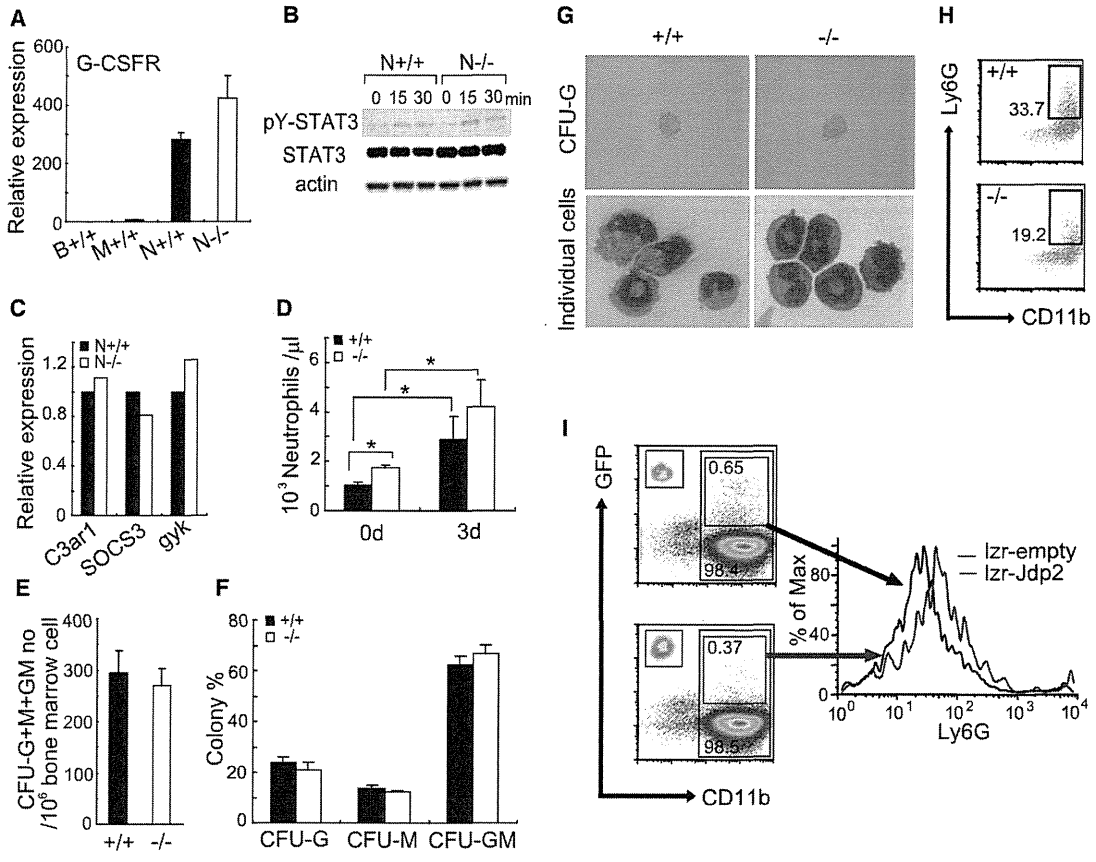

Figure 4. G-CSF Response Kinetics of *Jdp2*$^{-/-}$ Cells

(A) G-CSFR mRNA levels in wild-type and *Jdp2*$^{-/-}$ bone marrow CD11b^{+}Ly6C^{lo}Ly6G^{+} neutrophils (N+/+ and N−/−) measured by qPCR. Error bars, SE (n = 3).

(B) Cells in (A) were stimulated with 100 ng/ml G-CSF. STAT3 and pY-STAT3 levels were detected by immunoblotting.

(C) mRNA levels of STAT3 target genes in CD11b^{+}Ly6C^{lo}Ly6G^{+} neutrophils (N+/+ and N−/−) analyzed by a microarray.

(D) G-CSF (1 μg) was subcutaneously injected into wild-type and *Jdp2*$^{-/-}$ mice from days 0 to 3. At 6 hr after the last injection, blood was collected and CD11b^{+}Ly6G^{+} neutrophils were counted. Error bars, SE (n = 3). *p < 0.05.

(E and F) Bone marrow cells were cultured for 7 days in MethoCult. Total numbers of CFU-G, CFU-M, and CFU-GM colonies (E) and their rates (F) were determined. Error bars, SE (n = 6).

(G) Bone marrow cells were cultured for 7 days in MethoCult with 50 ng/ml G-CSF. Representative images of CFU-G and diaminobenzidine plus May-Grunwald-Giemsa-stained individual cells are indicated.

(H) CFU-G in (G) were collected and analyzed by FACS with CD11b and Ly6G markers.

(I) *Jdp2*$^{-/-}$ bone marrow cells were infected with a retrovirus encoding Jdp2 and GFP (Izr-Jdp2) or GFP alone (Izr-empty) with G-CSF for 9 days. CD11b^{+}GFP^{+} cells were gated and Ly6G expression levels were quantified by FACS. Gated cells were also sorted and stained by May-Grunwald-Giemsa (upper left insets in the scatter plots).

deficits, we performed in vitro killing assays with *S. aureus* and *C. albicans* (Figures 3O and 3P). Phagocytosis-dependent intracellular killing was inhibited by pretreating neutrophils with cytochalasin D. We observed that component killing mainly occurred in the extracellular space (Figures 3O and 3P) and that whole and extracellular bacterial killing by neutrophils from *Jdp2*$^{-/-}$ mice was significantly decreased compared with wild-type mice (Figures 3O and 3P). Together, these results clearly indicate that the bactericidal function is impaired in *Jdp2*$^{-/-}$ neutrophils.

Abnormal Differentiation of *Jdp2*$^{-/-}$ Neutrophils In Vitro Is Corrected by Re-expression of Jdp2

To investigate whether G-CSF signaling is altered by Jdp2 deficiency, we examined the expression levels of G-CSF receptor and STAT3. We found that G-CSF receptor (G-CSFR) expression was comparable between wild-type and *Jdp2*$^{-/-}$ neutrophils (Figure 4A), as was the expression of both STAT3 and phosphorylated STAT3 (Figure 4B). Microarray data confirmed the normal expression levels of G-CSF target genes (Figure 4C). We also counted the blood neutrophil numbers after intraperitoneal G-CSF injection and found comparable increasing rates of neutrophil numbers between wild-type and *Jdp2*$^{-/-}$ mice (Figure 4D). Thus, loss of Jdp2 does not influence G-CSF signaling.

Subsequently, we examined whether the altered differentiation of neutrophils in *Jdp2*$^{-/-}$ mice was a late-phase abnormality. *Jdp2*$^{-/-}$ bone marrow cells gave rise to the same numbers of granulocyte colony-forming units (CFU-G), granulocyte-macrophage colony-forming units (CFU-GM), and macrophage